Computational Study of the Rare Gas Fluorohydrides, Cyanohydrides, and Isocyanohydrides: Structures, Reactions, and Electronic Spectra

by

Miriam van Hoeve

A thesis submitted in partial fulfillment of the requirements for the degree of

Master of Science

Department of Chemistry
University of Alberta

Abstract

Little work on the electronic excited states of the family of HRgY (where Rg = rare gas and Y = electronegative group) compounds exist. There are two problems that are studied. The first is work aimed at extending the HRgY excited state area of research to include more work done on the electronic excited states of HRgF (where Rg = Ar, Kr, Xe, Rn) at the time-dependent density functional theory (TDDFT) level of theory. The effects of the Rg matrix and relativistic effects on the electronic spectra were investigated with scalar relativistic effects and spin-orbit coupling. The matrix caused the excitation energies to blue-shift (for all HRgF) and scalar relativistic effects caused them to red-shift (most significantly for HRnF). Spin-orbit coupling in HRnF altered its electronic spectrum significantly. A brief investigation of the computational efficiency of model core potentials (MCPs) in comparison to all-electron (AE) basis sets was done and it was found that MCP basis sets speed up excited state calculations while still giving similar results as the AE basis sets. The second problem addressed is the low-lying excited states (with spin-orbit coupling), structure, and reactions of HRnY and HXeY (where Y = CN, NC), specifically their isomerization and dissociation reactions. Isotopic substitution on reaction rates and the effectiveness of several pseudopotential basis sets was also studied for these systems. The work was done at the DFT, TDDFT, and Møller-Plesset (MP2) levels of theory.

Preface

The research related to the electronic spectra of the HRgF (where Rg = Ar, Kr, Xe, Rn) compounds has been published as M.D. van Hoeve and M. Klobukowski "Computational study of the electronic spectra of the rare gas fluorohydrides HRgF (Rg = Ar, Kr, Xe, Rn)," J. Phys. B. vol. 51, 055103, 2018 (10pp). M. Klobukowski was responsible for the spin-orbit coupling calculations. M.D. van Hoeve was responsible for all other data collection and analysis and writing of the manuscript. M. Klobukowski assisted with data collection and analysis and edited the manuscript. This work appears in Chapter 3.

The research related to the structure, reactions, and electronic spectra of HRgCN and HRgNC (Rg = Xe or Rn) is to be published as M.D. van Hoeve and M. Klobukowski "Structure, reactions, and electronic spectra of HRgCN and HRgNC (Rg = Xe or Rn)". Both M.D van Hoeve and M. Klobukowski were responsible for the data collection and analysis. M. Klobukowski was responsible for the spin-orbit coupling calculations. M.D. van Hoeve was responsible for writing the manuscript and M. Klobukowski edited the manuscript. This work appears in Chapter 4.

Table of Contents

List of Tables

List of Figures

Abbreviations

6Rc stands for six primitive Gaussian functions used in each symmetry where R = Rydberg functions and c = centre as there are 6 diffuse Rydberg functions placed on the centre of the system.

ADF Amsterdam density functional.

AE all-electron.

AO atomic orbital.

ccp cubic closed-packed.

CCSD(T) coupled cluster single-double and perturbative triple.

CPU central processing unit.

DFT density functional theory.

DK-SOC Douglas-Kroll spin orbit coupling.

DKH Douglas-Kroll-Hess.

DS double substituted.

FWHM full width at half maximum.

GAMESS the General Atomic and Molecular Electronic Structure System.

GGA generalized gradient approximation.

HF Hartree-Fock.

HOMO highest occupied molecular orbital.

ims2 IMCP-SR2.

ims3 IMCP-SR3.

IR infrared.

KIE kinetic isotope effect.

LDA local-density approximation.

LUMO lowest unoccupied molecular orbital.

MCP modal core potential.

mcpt, MCPt MCP-TZP, mcp-tzp, or MCP-tzp.

MO molecular orbital.

MP Møller-Plesset.

MRCI multireference configuration interaction.

Rg rare gas.

SAPt non-relativistic Sapporo-TZP-2012.

SAPtDK Sapporo-DKH3-2012.

SOC spin orbit coupling.

spkq, SPKQ SPKrQZP.

spkt, SPKT SPKrTZP.

SR scalar relativistic.

SS single substituted.

TDDFT time dependent density functional theory.

TZP triple-zeta plus polarization.

UV ultraviolet.

VUV vacuum ultraviolet.

VWN Vosko, Wilk, Nusair.

zfk3 ZFK3-DK3.

zfk4 ZFK4-DK3.

ZORA scalar relativistic zero-order regular approximation.

ZPE zero point energy.

Chapter 1

Introduction

1.1 Motivation

Rare gases were long believed to be inert, but they do exhibit reactivity and form compounds. Researching rare gas compounds and their reactivity challenges the archaic idea of rare gas inertness [1]. Moreover, little work on the excited states of the HRgY (where Rg = rare gas and Y = electronegative group) family of compounds exists. Experimental and theoretical work for excited states has been done on HXeY (Y= Cl, Br, I, CN) but little work on the excited states of the HRgY compounds exists beyond that [2, 3]. Moreover, doing experimental work on compounds of radon is difficult as this element is highly radioactive. Radon is hazardous to work with and decays quite quickly via α decay with a half-life of 3.8 days for its most stable isotope radon-222 [4]. Therefore, studying radon compounds theoretically is desirable. For example, work on the thermochemistry of the HXeNC to HXeCN exists while that of HRnNC to HRnCN does not [5]. Studying the radon case may still be interesting as radon compounds tend to experience relativistic effects. Because of their relativistic effects, the radon compounds are expected to have slightly different properties, such as electronic spectra, than the lighter rare gas compounds of the same family.

1.2 Thesis objectives

This works aims to extend the work on excited states for the family of rare gas compounds of the form HRgY. The molecular orbitals involved in the transitions of the main peaks in their electronic spectra are of interest. For the excited state calculations in Chapter 3, we want to see how our chosen methods and basis sets perform in the excited state calculations for these rare gas system [6]. Of interest is how the model core potential basis sets behave relative to all electron basis sets. The influence relativistic effects (both scalar relativistic and spin-orbit coupling) have on the electronic spectra is also investigated, mostly for the radon compounds as radon is a heavy atom and is expected to have the greatest relativistic effects. For the geometry optimizations and thermochemistry in Chapter 4, it is of interest to see how the basis set ims3 performs relative to the cheaper ims2 basis set and the more expensive zfk3 and zfk4 basis sets [7]. The dissociation and isomerization of HRgCN and HRgNC (Rg = Xe, Rn) is also of great interest as well as the kinetic isotope effects of these reactions.

Chapter 2

Background

2.1 Rare gas history

Compounds containing rare gas atoms were thought to be non-existent due to the believed inertness of the rare gas elements. In 1933, Linus Pauling suggested the possible existence of Xenic acid, KrF_6 and XeF_6 [8]. Xe compounds were the first to be synthesized as Xe was most likely to form compounds due to its large polarizability and lower ionization energy. Unlike Rn, Xe is not radioactive and so less hazardous to work with. In 1962, Neil Bartlett at the University of British Columbia synthesized the first rare gas compound, $Xe^+[PtF_6]^-$ (xenon hexafluoroplatinate), an orange-yellow solid, from PtF_6 (red vapour) and Xe [9]. He came to this conclusion by observing that PtF_6 reacts with O_2^+ to yield $O_2^+[PtF_6]^-$. Since the first ionization energy of Xe is similar to that of O_2^+, he predicted the possibility of synthesizing $Xe^+[PtF_6]^-$ in a similar manner. Although there is some work suggesting that Bartlett's experiment did not produce the $Xe^+[PtF_6]^-$ compound (it was more likely to be $[XeF]^+[PtF_6]^-$), Bartlett's research was pioneering work on the synthesis of rare gas compounds as within a few months XeF_2 and XeF_4 were synthesized by others [10–12].

A common type of rare gas compound is HRgY where Rg = rare gas atom and Y = electronegative group [13]. The first Ar compound was of this type, HArF, and was synthesized by Khriachtchev *et al.* [14]. HRgY tend to be metastable compounds

[13]. The HRg bond is covalent while the bond between the fragments HRg^+ and Y^- is mostly ionic. These compounds are formed by photolyzing HY with UV light in a rare gas matrix which then leads to the thermal activation of the H atoms. Work has been done on the HRgY family, especially focusing on their IR spectra [15, 16], in which the stiff HRg bond creates an infrared (IR) peak at around 2000 cm^{-1} and it is this peak that is used in its identification.

2.2 Methods

2.2.1 HF and MP2

The energy and properties of a system may be obtained by solving the Schrödinger equation (equation 2.1)

$$\hat{H}(1,2,...,N;\{R\})\Psi(1,2,...,N;\{R\}) = \mathcal{E}(\{R\})\Psi(1,2,..,N;\{R\}). \tag{2.1}$$

The wavefunction Ψ (equation 2.2) is antisymmetric for electrons and other fermions (equation 2.2)

$$\Psi(1,2,...,N) = -\Psi(2,1,..,N), \tag{2.2}$$

where $\hat{H}$ is the Hamiltonian (energy operator), $\mathcal{E}$ is energy, Ψ is the wavefunction that depends on 4N variables. The 4N variables are $(x_i, y_i, z_i, \sigma_i)$ where x_i, y_i, z_i are the space coordinates and σ_i is the spin coordinate. The quartet of symbols x_i, y_i, z_i, σ_i is abbreviated as i. The positions of the nuclei $\{R\}$ are assumed to be fixed under the Born-Oppenheimer approximation.

The restricted Hartree-Fock method (HF) is a simple method for obtaining the energy and other properties of a many-body system (compound) via approximating the wavefunction of the system (Ψ) with a single Slater determinant (Φ) built from spin orbitals (equation 2.3, where ψ denotes a spin orbital) [17–22],

$$\Phi(1,2,...,N) = |\psi_1(1)\psi_2(2)...\psi_N(N)|. \tag{2.3}$$

HF theory contains no correlation effects other than from same spin electrons. The variational method (equation 2.4) is used to get the equations for the spin orbitals which are then solved to obtain the wavefunction and energy of the system,

$$\langle \hat{H} \rangle = \langle \Phi | \hat{H} | \Phi \rangle = E \geq \mathcal{E}. \tag{2.4}$$

In equation 2.4, E is the variational energy which will always be greater (although can come close to) the exact energy, $\mathcal{E}$. The spin orbitals used to construct Φ are optimized so that E is minimized and therefore is close in value to exact value $\mathcal{E}$. The energy may be evaluated as the integral in equation 2.5,

$$E = \frac{\int \Phi^*(1,2,...,N)\hat{H}(1,2,...,N)\Phi(1,2,...,N)d\xi_1...d\xi_N}{\int \Phi^*(1,2,...,N)\Phi(1,2,...,N)d\xi_1...d\xi_N}. \tag{2.5}$$

The spin orbitals $\psi(x,y,z)$ are defined as products of orbitals $\phi(x,y,z)$ and the Pauli spin functions $\alpha(\sigma)$ and $\beta(\sigma)$ (equation 2.6 and 2.7),

$$\Psi_i(x,y,z,\sigma) = \phi_a(x,y,z)\alpha(\sigma) \tag{2.6}$$

$$\Psi_j(x,y,z,\sigma) = \phi_a(x,y,z)\beta(\sigma). \tag{2.7}$$

The orbitals ϕ_a are the solutions of the Hartree-Fock equations (equation 2.8)

$$\hat{f}(x,y,z)\phi_a(x,y,z) = \epsilon_a \phi_a(x,y,z). \tag{2.8}$$

The Møller-Plesset (MP) perturbation theory is a method that builds on the HF method by adding electron correlation (HF only accounts for the electron correlations due to same spin electrons) [23]. The MP perturbation theory can be done at the second, third, and fourth order (MP2, MP3, MP4, respectively) [24–26]. Equation 2.9 shows the Hamiltonian used in the MP2 method ($\hat{H_{MP}^{(0)}}$)

$$\hat{V} = \hat{H} - \hat{H}_{MP}^{(0)}, \tag{2.9}$$

where $\hat{H}$ is the full Hamiltonian (equation 2.1) and $\hat{V}$ is the perturbation.

The correlation energy from the electron correlation is defined as equation 2.10,

$$E_{\text{corr}} = \mathcal{E} - E_{\text{HF}}. \tag{2.10}$$

Equation 2.10 shows that the MP method adds a perturbational correction (E_{corr}) to the HF energy via using the HF wavefunction. The difference between the exact energy $\mathcal{E}$ and the HF energy is called the electron correlation energy.

2.2.2 DFT and TDDFT

Density functional theory (DFT) is another method for calculating the electronic structure and energy of a ground state system, but unlike MP it does not involve improving on the HF method [27]. This method uses functionals of electron density (equivalent to the wavefunction) which is a function that depends on the function of the spatial coordinates,

$$E = \mathcal{F}[\rho(x, y, z)]. \tag{2.11}$$

The energy can be calculated from the electron density (ρ) and an unknown functional ($\mathcal{F}$) as shown in equation 2.11. x, y, z is a single point for all the electrons in the system. The first Hohenberg-Kohn theorem states that the properties of a system can be obtained through the electron density. The second Hohenberg-Kohn theorem states that the total energy of a system should be minimized through equation 2.11.

In the DFT method, there is the Kohn-Sham equation (equation 2.12) which is similar to the HF equation or the Schrödinger equation,

$$\hat{F}(x, y, z)\phi_i(x, y, z) = \epsilon_i\phi_i(x, y, z). \tag{2.12}$$

It contains the Kohn-Sham operator ($\hat{F}$), the Kohn-Sham orbital energies (ϵ_i) and orbitals (ϕ_i) which are used to define the electron density. The functional is a functional of the electron density but the exact functional to the Kohn-Sham equation is not known so approximations are used. The Kohn-Sham operator also contains the exchange-correlation term. The exchange accounts for electron antisymmetry and the

correlation accounts for electron correlation. The exchange-correlation term is also separated.

Many different exchange-correlation functionals exist for the DFT method. A specific type of functional is the hybrid functional. They are called hybrid because they contain part of the HF operator: a portion of the HF exact exchange is put into the exchange-correlation functional. Some examples of hybrid functionals are: PBE0, B2PLYP, B3LYP, CAMB3LYP, and CAMYB3LYP [28, 31–33] while B2PLYP is a double hybrid [29, 30]. B3LYP stands for Becke 3-parameter exchange and Lee-Yang-Parr correlation functional [31]. B3LYP contains three parameters that mix: the Becke 88 exchange functional, the correlation functional of Lee, Yang and Parr, and the VWN (Vosko, Wilk, Nusair) local-density approximation (LDA) to the correlation functional. LDA functionals only depend on the density at a given point. PBE0 is a hybrid of the Perdew-Burke-Ernzerhof (PBE) exchange energy (full PBE correlation energy) and Hartree-Fock exchange energy in a 3:1 ratio [28]. The GGA functionals depends on the local density and the gradient of the density. B2PLYP has an hybrid-GGA part and a perturbative correlation part [29]. B2PLYP has exact exchange and GGA corrections with electron-electron and electron-nuclei energy [29, 30]. The excitation energies and the ground state orbitals are then used in a perturbative treatment which is then added to energies [29, 30]. CAMB3LYP is a combination of B3LYP but with long range corrections [32]. CAMB3LYP is an improvement to B3LYP because it results in better results for the charge transfer excitations [32]. CAMYB3LYP is similar to CAMB3LYP but it has a different switching function, which is the Yukawa potential switching function [33].

TDDFT (time-dependent density functional theory) is a DFT method; TDDFT is time-dependent so it can be used to calculate excited electronic states (a time-dependent problem) and from there generate the electronic spectrum [35, 36].

2.3 Basis sets

The molecular orbitals are built from a linear combination of basis functions. These basis functions are termed the basis set. Table 2.1 shows the basis sets and their abbreviations used in this thesis.

Table 2.1: Basis sets and their references.

name	type[a]	abbreviation	reference
IMCP-SR2	MCP	ims2	[37]
IMCP-SR3	MCP	ims3	unpublished
MCP-TZP	MCP	mcpt	[38]
ZFK3-DK3	MCP	zfk3	[39]
ZFK4-DK3	MCP	zfk4	[39]
SPKrTZP	AE	spkt (sapt)	[40, 41]
SPKrQZP	AE	spkq	[40, 41]
PolX	AE	polx	[42–46]
QZ4P[b]	AE	qz4p	[47]

[a] MCP = model core potential, AE = all electron. [b] Slater functions.

The basis sets used are ims2, ims3, zfk3, zfk4, spkt (also called sapt in Chapter 3), spkq, mcpt, polx, and qz4p [37–42, 47]. ims2, ims3, mcpt, zfk3 and zfk4 are basis sets that contain model core potentials. zfk3 and zfk4 contain both scalar Douglas-Kroll (DK) and spin orbit coupling (SOC) relativistic effects [39]. zfk3 contains the diffuse functions from aug-cc-pVTZ and zfk4 contains the diffuse functions from aug-cc-pVQZ [39]. spkt (triple zeta valence meaning three basis functions per each valence orbital) and spkq (quadruple zeta valence) are basis sets with relativistic effects included that belong to the class of Sapporo basis sets [40, 41]. mcpt is a model core potential basis set [38]. The polx basis set was designed for polarizability studies [42–46]. The qz4p is a quadruple zeta all electron Slater basis set with four

polarization functions [47].

It is common to augment basis sets with diffuse functions in order to better describe the far end of an orbital; these functions have very small exponents.

A specific set of diffuse functions is based on the even-tempered expansion [48–50]. These are often used to describe anions and Rydberg states. In the Rydberg states, these are very diffuse molecular orbitals that resemble really big atomic orbitals. The electron is so far out that it sees the molecule as a point, H-like, and therefore resides in the H-like atomic orbitals.

2.4 Relativistic effects

Relativistic effects occur with atoms when an electron approaches the speed of light (c). The mass of the electron may increase due to how close it travels to the speed of light as seen in equation 2.13

$$m_v = \frac{m_0}{\sqrt{1-(v/c)^2}}, \tag{2.13}$$

where m_0 is the mass of the particle (in this case an electron) at rest and m_v is the mass of the particle moving at a speed of v.

The high speed increases the electron's mass, making the s and p orbitals contract (direct effect). The d and f orbitals expand due to increased shielding of the nucleus due to the contraction of the inner subshells (indirect effect). The heavier the nucleus, the greater the relativistic effects and so relativistic effects are more prominent in heavier atoms. The bond lengths tend to contract (relativistic contraction) for atoms down a group unless lots of d and f atomic orbitals (or molecular orbitals composed of d and f orbitals) are involved, in which case bond lengths extend. The two types of relativistic treatments used in this thesis are scalar relativistic and spin-orbit coupling. Spin-orbit coupling is the interaction of the electron's spin angular momentum with its orbital angular momentum. This may cause splitting and shifting in the electronic spectrum of a system.

The relativistic version of the Schrödinger equation is the Dirac equation (equation 2.14) where i is the imaginary unit, m_e is the rest mass of an electron, and α_i are matrices,

$$i\hbar\frac{\partial\Psi}{\partial t} = [-ic\hbar(\alpha_1\frac{\partial}{\partial x_1} + \alpha_2\frac{\partial}{\partial x_2} + \alpha_3\frac{\partial}{\partial x_3}) + m_e c^2]\Psi. \tag{2.14}$$

The Dirac equation is the foundation of various approximate relativistic quantum chemistry methods (e.g. scalar relativistic zero-order regular approximation (ZORA) and Douglas-Kroll-Hess (DKH)).

2.5 Thermochemistry and kinetic isotope effects

In order to obtain thermochemical data, geometry optimizations and harmonic vibrational analysis are performed for the reactant, product, and transition state. In geometry optimization, a series of iterations is done until a stationary point is found, where the gradient is close to zero. Potential energy surfaces contain stationary points that correspond to products, reactants, and saddle points (which are maxima in one direction but minima in all other directions) which correspond to transition states. Information about all energy levels (electronic, vibrational, rotational, and translational) at the stationary points may be used to compute values of thermodynamic functions via the formalism of statistical thermodynamics.

In order to obtain G (the free energy of a system), the wavefunction of a molecule can be written as equation 2.15 so that the E_{total} is given in equation 2.16, the partition function (Q) in equation 2.17, and then G_{total} is defined in equation 2.18

$$\psi_{total} = \psi_{translation}\psi_{rotation}\psi_{vibration}\psi_{electronic} \tag{2.15}$$

$$E_{total} = E_{translation} + E_{rotation} + E_{vibration} + E_{electronic} \tag{2.16}$$

$$Q_{total} = Q_{translation}Q_{rotation}Q_{vibration}Q_{electronic} \tag{2.17}$$

$$G_{total} = G_{translation} + G_{rotation} + G_{vibration} + G_{electronic}. \tag{2.18}$$

The partition functions for the translation, rotation, vibration, and electronic states can be obtained with equation 2.19 where g is the degeneracy of the state, κ_B is the Boltzmann constant, T is temperature, and p = total, translation, rotation, and electronic

$$Q_p = \sum_{\text{states}} g_p(\frac{-E_p}{\kappa_B T}). \tag{2.19}$$

G is also obtained with equation 2.20 where N (the number of indistinguishable molecules) is usually Avogadro's number,

$$G_p = -N\kappa_B T \ln \frac{Q_p}{N}. \tag{2.20}$$

The kinetic isotope effect (KIE) arises when one atom of a reactant is substituted with a heavier isotope, e.g. by replacing hydrogen with deuterium [51]. Because of the change in mass, the vibrational energy states change (as well as the zero point energy (ZPE)) and so the reaction rate constant changes. This change in rate is the kinetic isotope effect. The KIE is a ratio of the rate constants (taken to be heavy over light in this thesis) before and after the isotopic substitution as shown in equation 2.21:

$$\frac{k_H}{k_L} = \frac{Q_H^{\ddagger} Q_L^R}{Q_L^{\ddagger} Q_H^R} \exp \frac{-(\delta E_0^R - \delta E_0^{\ddagger})}{RT}, \tag{2.21}$$

where k_L is the rate constant, $Q^{\ddagger}$ is the partition function of the transition state, Q^R is the partition function of the reactant, $\delta E_0^{\ddagger}$ is the difference between the ZPEs of the isotopic transition state and the original transition state, δE_0^R is the difference between the ZPEs of the isotopic reactant and the original reactant, R is the gas constant, T is temperature (in K), the H subscript denotes the (heavier) isotopically substituted system, and L subscript denotes the original (lighter) system. The magnitude of KIEs may help reveal which bonds are involved in the reaction. Primary KIE is when the bond that is broken is attached to the isotopically substituted atom, resulting in a KIE less than 1 ($k_H < k_L$). When the substituted atom is located further away from the bond being broken, the KIE is close to 1 ($k_H \approx k_L$) and is termed the secondary isotope effect.

2.6 Software and hardware

GAMESS-US [52] and ORCA [53, 54] are program packages that use Gaussian basis functions and that can run calculations for methods such as HF, MP2, DFT, and TDDFT on chemical systems in order to obtain properties such as optimized geometries, total energies, molecular orbital (MO) energies, and electronic excitation energies. Amsterdam Density Functional (ADF) is a program that uses Slater basis functions and the DFT method (including TDDFT) [55]. This program was used because it allows for excited state calculations with spin orbit coupling. GAMESS-US currently lacks the SOC capability for excited states using TDDFT.

Chapter 3

Computational study of the electronic spectra of the rare gas fluorohydrides HRgF (Rg = Ar, Kr, Xe, Rn)

3.1 Introduction

The first argon-containing compound synthesized was HArF, prepared in 2000 by Khriachtchev *et al.* who synthesized it via the photolysis of HF in a solid argon matrix using a vacuum-UV lamp [14]. IR spectroscopy was used to confirm its existence [14]. In 2001, HKrF was synthesized and characterized in a similar way as HArF [56]. To our current knowledge, HXeF and HRnF have yet to be synthesized [13].

The photodecomposition of HArF and HKrF was studied experimentally and theoretically [14, 56–58]. Some excited states of HArF are repulsive and lead to its photodissociation [14]. Properties of HArF and HKrF in their respective matrices were studied computationally and experimentally [56, 59–62]. Two different conformations of HRgF in its cluster exist: double substituted (DS) and single substituted (SS) [61, 62].

The vibrational spectra of HRgF (Rg = He, Ne, Ar, Kr, Xe, Rn) with anharmonic corrections were computed by Lundell *et al.* at the MP2 and CCSD(T) levels of theory [15]. The stiff HRg bond created a peak at around 2000 cm^{-1} [63]. This spectrum

was used by Khriachtchev *et al.* to identify HKrF [56, 63]. The IR spectrum of HArF closely matched the experimental spectrum, but small discrepancies existed due to matrix effects [14, 63].

The vibrational spectra of HRgF (Rg = Ar, Kr), in their respective matrices, were studied theoretically by Gerber *et al* [16, 63]. The vibrational peaks of HRgF in its rare gas cluster are shifted relative to the vibrational peaks of free HRgF [16, 63]. The shifts might be due to the large charges on the atoms in HRgF that interact with the atoms in the matrix [16]. To a lesser degree, induced dipole moments could also contribute to these shifts [16, 62].

Fitzsimmons *et al.* studied the HRgF (Rg = Ar, Kr, Xe, Rn) systems where the model core potential (MCP) method was compared to an approach using all-electron (AE) basis sets [64]. Furthermore, Fitzsimmons *et al.* identified the MCP basis set that was the most efficient and gave the best results for HXeY and HRnY (Y = halogen) [65].

The model core potential method replaces the core electrons with a potential, while still retaining the nodal structure of the valence orbitals [7, 66, 67]. An important feature of MCPs is that they account for relativistic effects [7, 66, 67]. The model core potential triple-zeta plus polarization (MCP-tzp) basis set is rarely used in excited state calculations. We included the MCP-tzp basis set in this project to study its accuracy and efficiency for excited state calculations on rare gas systems.

Experimental and theoretical studies on the excited states and vacuum-UV (VUV) spectra of HXeY (Y = Cl, Br, I, CN) have been done [2, 3]; however, experimental VUV spectra of HRgF (Rg = Ar, Kr, Xe, Rn) have not yet been obtained. The predicted spectrum could be used to distinguish HRgF from its by-products and environment in an experimental electronic spectrum of HRgF. As the experimental spectra of HArF and HKrF would be recorded in a rare gas matrix, studies of the excited states of HArF and HKrF in their rare gas matrix ($HArF@Ar_{12}$ and $HKrF@Kr_{12}$) were done, in addition to the gas-phase modelling. The matrix could alter the elec-

tronic spectra just as it shifted the vibrational spectra. Both the efficacy of the MCPs and the role of relativistic effects on the spectra of HRgF were also investigated.

In this chapter, the electronic spectra of HRgF (where Rg = Ar, Kr, Xe, Rn) are presented. As well as HArF and HKrF in their respective rare gas matrix ($HArF@Ar_{12}$ and $HKrF@Kr_{12}$) as the matrix is expected to shift the spectra. The evaluation of how well the MCP basis set behaved in excited state calculations is also presented. In the MCP method, the core is replaced with a potential while still retaining the nodal structure. Pseudopotential methods are much faster than all electron basis sets. The performance of the MCP was measured relative to all electron basis sets, in these rare gas excited state calculations. Lastly, the relativistic effects on the electronic spectra is presented, especially for that of HRnF which contains the heaviest rare gas atom.

3.2 Methods and procedure

The geometry of all systems was calculated by Fitzsimmons *et al.* using the MP2 and the MCP-TZP basis set [64]. The bond lengths in these linear molecules were:

r_e(Ar-H) = 1.304 Å, r_e(Ar-F) = 1.954 Å for HArF [68], r_e(Kr-H) = 1.456 Å, r_e(Kr-F) = 2.034 Å for HKrF [68], r_e(Xe-H) = 1.633 Å, r_e(Xe-F) = 2.100 Å for HXeF [68], and r_e(Rn-H) = 1.736 Å, r_e(Rn-F) = 2.175 Å for HRnF [68]. For the linear HRgF molecules the C_{2v} subgroup of $C_{\infty v}$ was used in computations.

Singlet excited states were computed using the time-dependent density functional theory (TDDFT) [69, 70], as implemented in GAMESS-US [52]. Both all-electron and pseudopotential basis sets were used. The all-electron basis sets included Sadlej's PolX6Rc and PolXDK6Rc as well as Sapporo SAPt6Rc and SAPtDK6Rc basis sets. PolX denotes the non-relativistic basis set designed for polarizability studies [42, 43], PolXDK is the Douglass-Kroll-Hess second-order (DKH2) version of the PolX basis set, SAPt stands for the non-relativistic Sapporo-TZP-2012 [71], and SAPtDK denotes its relativistic counterpart, Sapporo-DKH3-TZP-2012 basis [40, 41]. The MCP basis set was MCPt6Rc which employs a potential that models the core electrons,

where MCPt stands for MCP-TZP [38]. All the relativistic basis sets were used with the DKH2 approximation [72, 73].

All basis sets contained a set of spherical even-tempered [50] s-, p-, and d-type diffuse functions that were positioned on the rare gas atom in order to describe the Rydberg states of HRgF; six primitive Gaussian functions were used in each symmetry. This set of diffuse functions was denoted by the string 6Rc in the abbreviated basis set name. Occasionally, the diffuse function exponents were too close to those in the original basis set; in such cases, some of the s function and p functions were deleted to avoid linear dependencies. The basis sets used are shown in table 3.1 and their spatial extent is illustrated in figures 3.1 – 3.6. Adding more diffuse functions to the rare gas atom did not improve results. Addition of diffuse functions to the hydrogen and fluorine atoms increased the excitation energies by about 0.1 eV, at the cost of increasing the CPU time by a factor of five, and these functions were not used.

Table 3.1: Even-tempered diffuse functions used in all the calculations.

gaussian type	exponents
on Ar	
s type	0.0733687, 0.0275474, 0.0103425, 0.0038825, 0.0014576, 0.0005471
p type	0.0527741, 0.0180255, 0.0061568, 0.0021027, 0.0007184, 0.0002441
d type	0.1340495, 0.0438249, 0.0143254, 0.0046822, 0.0015293, 0.0005002
on Kr	
s type	0.0600558, 0.0249034, 0.0103271, 0.0042823, 0.0017755, 0.0007356
p type	0.0429426, 0.0156774, 0.0057233, 0.0020889, 0.0007621, 0.0002775
d type	0.1117751, 0.0415609, 0.0154538, 0.0057444, 0.0021342, 0.0007935
on Xe	
s type	0.0526728, 0.0277110, 0.0145784, 0.0076691, 0.0040348, 0.0021225
p type	0.0310495, 0.0126782, 0.0051768, 0.0021139, 0.0008630, 0.0003520
d type	0.0945632, 0.0413764, 0.0181056, 0.0079204, 0.0034664, 0.0015149
on Rn	
s type	0.0471382, 0.0217740, 0.0100568, 0.0046452, 0.0021450, 0.0009908
p type	0.0259346, 0.0110411, 0.0047003, 0.0020011, 0.0008516, 0.0003624
d type	0.0753842, 0.0332235, 0.0146413, 0.0064534, 0.0028427, 0.0012520

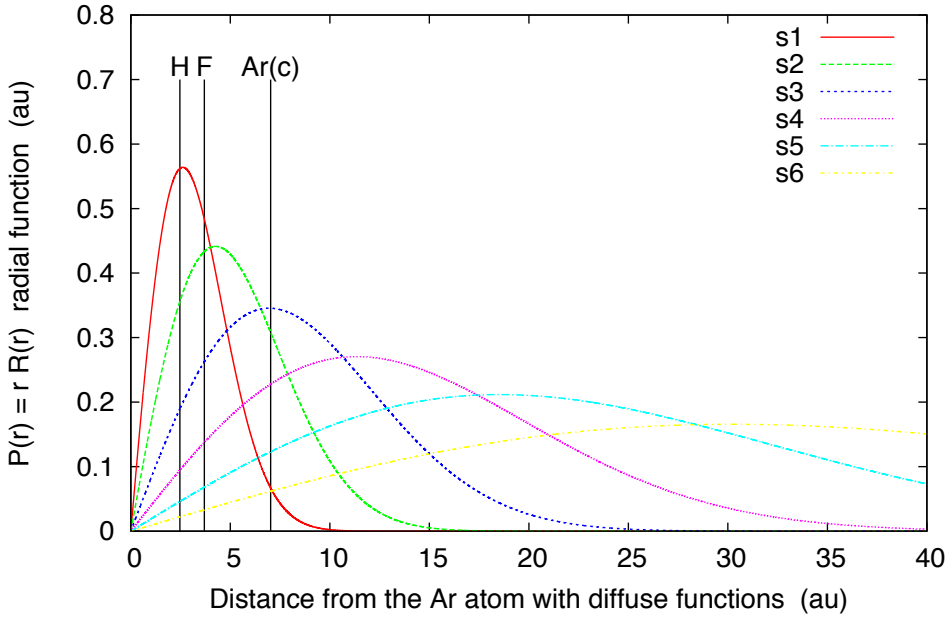

Figure 3.1: Ar diffuse s-type radial functions. Ar-H = 2.464, Ar-F = 3.692, and Ar-Ar(c) = 7.023 au.

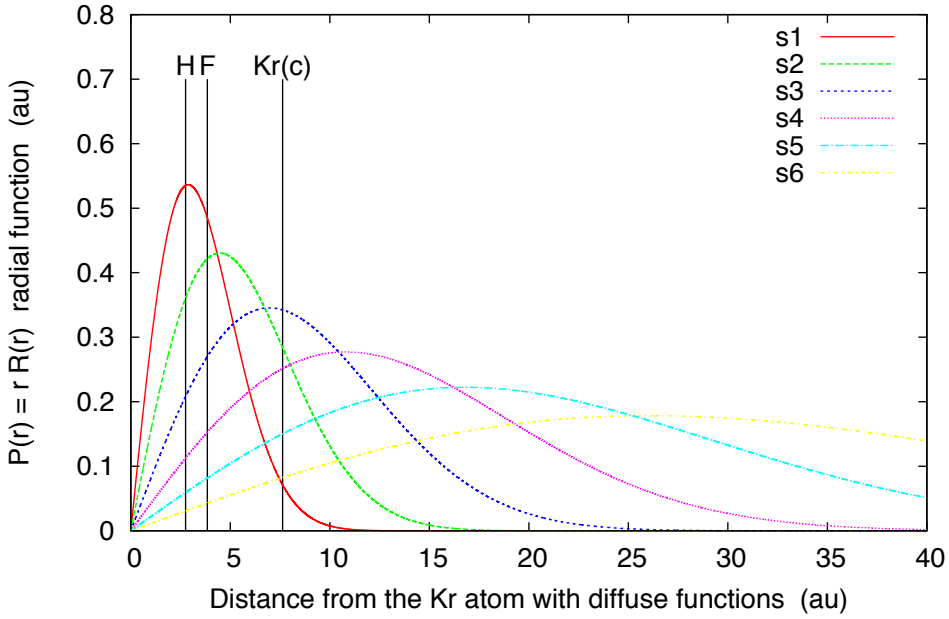

Figure 3.2: Kr diffuse s-type radial functions. Kr-H = 2.751, Kr-F = 3.844, and Kr-Kr(c) = 7.625 au.

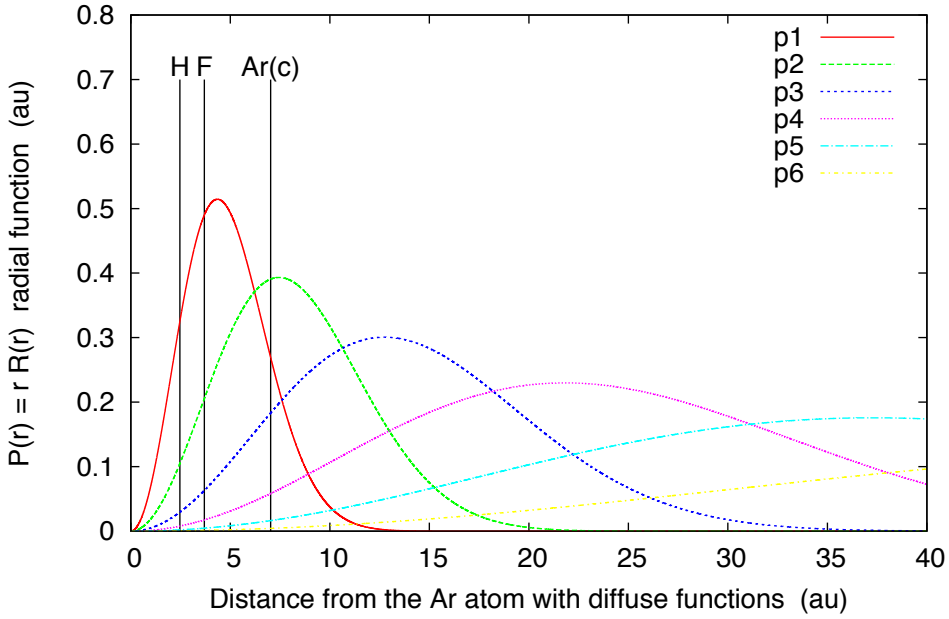

Figure 3.3: Ar diffuse p-type radial functions. Ar-H = 2.464, Ar-F = 3.692, and Ar-Ar(c) = 7.023 au.

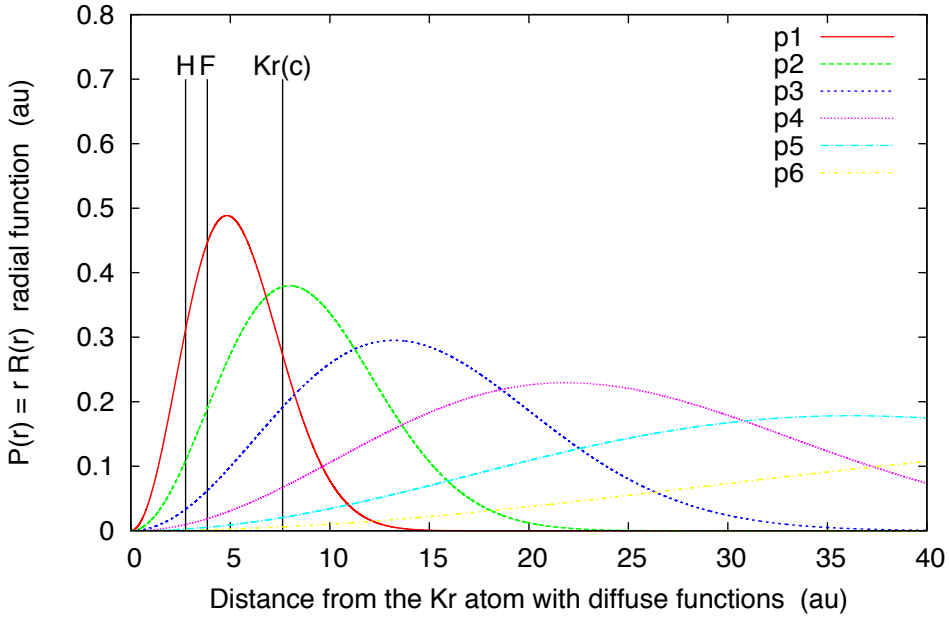

Figure 3.4: Kr diffuse p-type radial functions. Kr-H = 2.751, Kr-F = 3.844, and Kr-Kr(c) = 7.625 au.

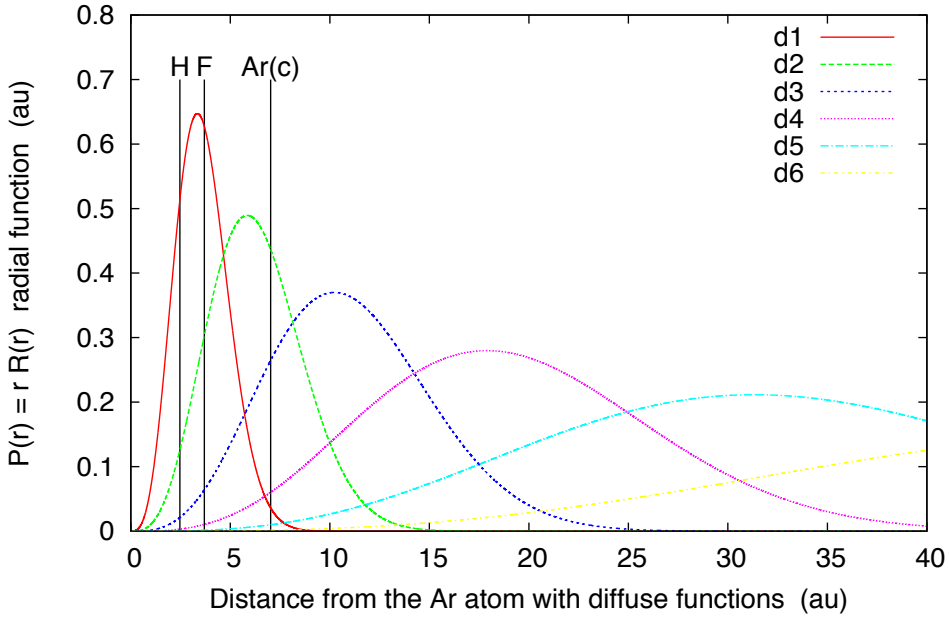

Figure 3.5: Ar diffuse d-type radial functions. Ar-H = 2.464, Ar-F = 3.692, and Ar-Ar(c) = 7.023 au.

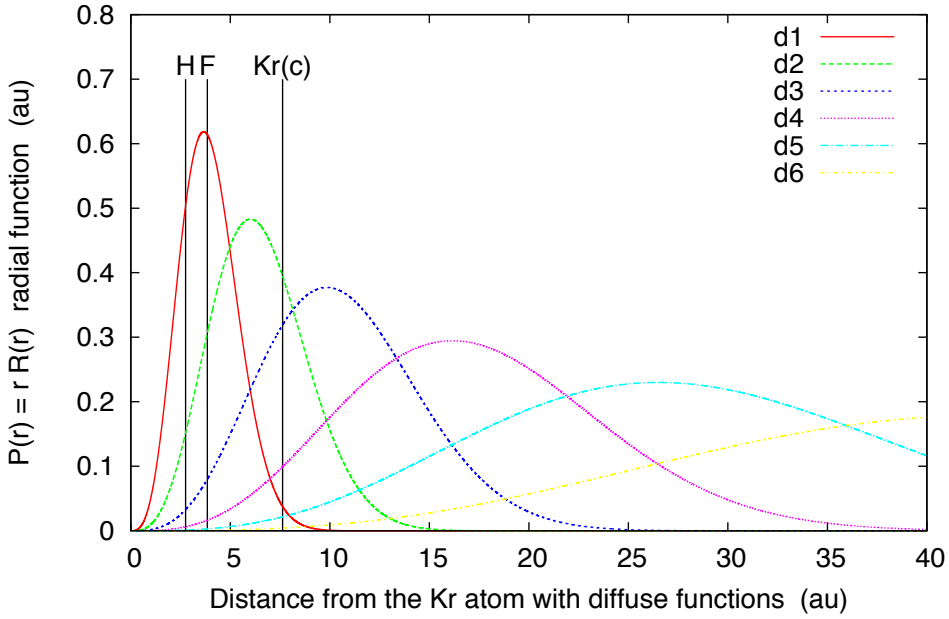

Figure 3.6: Kr diffuse d-type radial functions. Kr-H = 2.751, Kr-F = 3.844, and Kr-Kr(c) = 7.625 au.

Most of the TDDFT work was carried out using GAMESS-US in order to employ the MCP-TZP basis set. The CAMB3LYP functional was used as it was shown to be one of the best functionals for the excited state calculations [32, 36]. The parameters used in the GAMESS calculations are shown in table 3.2. Additional work was done using Amsterdam Density Functional (ADF) program [55].

Table 3.2: Parameters used in all-electron GAMESS-US calculations

```
$system mwords=200 memddi=0 $end
$contrl qmttol=1.0d-6 itol=40 icut=14 inttyp=rysquad maxit=50
       scftyp=rhf    runtyp=energy
       tddft=excite  dfttyp=camb3lyp
       pp=NONE       ispher=1
$end
$basis
      basnam(1) = basH basKr basF
$end
$dft
       nrad=115  nleb=590  nrad0=115  nleb0=590
$end
$scf
       conv=1.0d-8 diis=.F. soscf=.T.
$end
$tddft cnvtol=1.0d-9 maxvec=100 ntrial=78
       nrad=115  nleb=590  nstate=30 iroot=1 mult=1
       tdPrp=.false. TPA=.false.
$end
```

Note: `pp=MCP` was used the MCP calculations.

The computations done with the PolX and PolXDK basis sets, which were designed to study electric properties in ground electronic states and were not optimized for excited state calculations [42], were done solely to study the scalar relativistic (SR) effects in the electronic absorption spectra of HRgF, and one should not expect them to give reliable excitation energies.

One of the objectives in this chapter was to evaluate the performance of MCPt6Rc basis sets in excited state calculations. Excitation energies obtained with SAPtDK6Rc basis sets were used for comparison with the MCPt6Rc results. The SAPtDK6Rc basis set was unavailable for Ar and SAPt6Rc was used instead for HArF. As the relativistic effects are expected to be minute in Ar, we would expect SAPt6Rc to yield

the same results as SAPtDK6Rc. PolX6Rc gave very similar results as PolXDK6Rc for HArF; therefore, using SAPt6Rc instead of SAPtDK6Rc for HArF is justified.

The excited states of HRgF@Rg_{12} (Rg = Ar, Kr) were calculated at the TDDFT/MCPt6Rc level of theory, with the MCPt basis being the most computationally efficient basis set among the basis sets used in this study. A cubic closed-packed (*ccp*) crystal structure was assumed for the Rg solids, with symmetry specified as C_{4v} and the configuration of HRgF@Rg_{12} taken as single-substituted (SS) [56, 59–62]. The cluster of twelve Rg (Rg = Ar, Kr) atoms was selected as the nearest neighbours of the Rg atom at the centre of the face in the *ccp* structure of the solid Rg (figure 3.7). The lattice constants were $a = 5.256$ Å for argon [74] and $a = 5.706$ Å for krypton [75]. To increase computational efficiency, the diffuse functions were added only to the basis set on the central Rg atom, to which H and F atoms were attached; the remaining twelve Rg atoms, constituting the matrix cluster, were described by an unaugmented MCPt basis set.

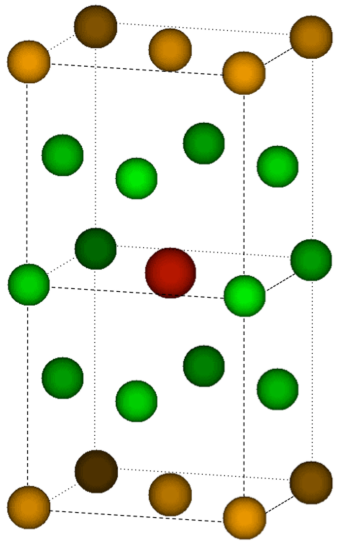

Figure 3.7: Orientation of argon atoms in the two units cells used to represent solid state confinement. The red dot in the centre represents the Ar atom with the diffuse functions, to which the H and F atoms will be attached. The green dots represent the Ar atoms that define the Ar cluster, and the brown dots represent the atoms that were ignored.

Spectra were simulated using the Cauchy-Lorentz line shape with a full width at half maximum (FWHM) of 0.075 eV. All calculations were carried out using Mac Pro and Linux computers available in our laboratory.

3.3 Results and discussion

3.3.1 Electronic spectra of HRgF

Figure 3.8 presents the VUV spectra of the HRgF systems obtained at the the level of TDDFT(CAMB3LYP) using the two families of all-electron basis sets and the MCP basis sets and shows that the Sapporo and MCP basis sets bring about results that are closer to each other than to those obtained with Sadlej's basis sets. The spectra obtained with the Sapporo and MCP basis sets are shown in greater detail in figures 3.9 – 3.16.

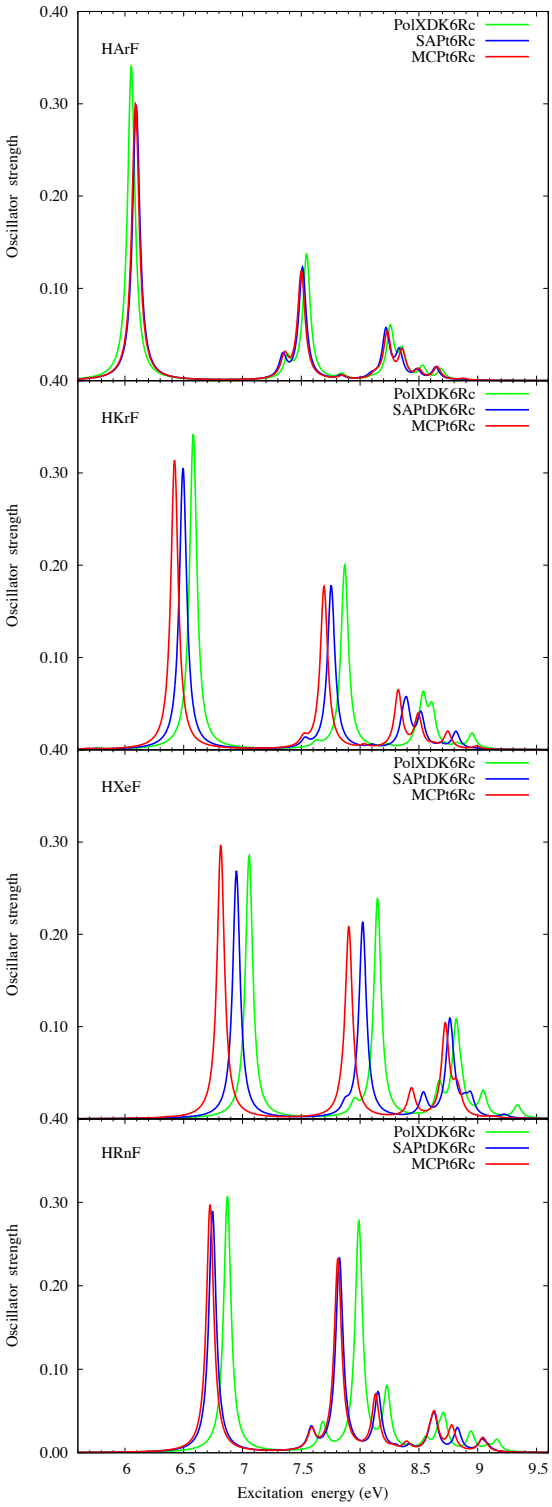

Figure 3.8: TDDFT(CAMB3LYP) spectra of the HRgF family

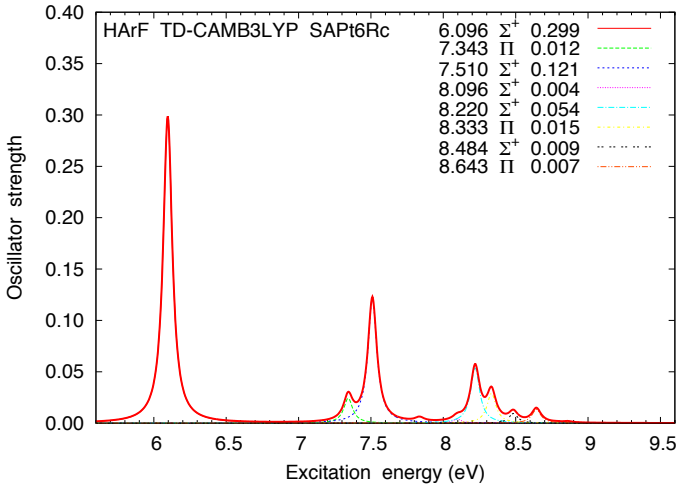

Figure 3.9: HArF singlet absorption spectrum simulated with Cauchy-Lorentz functions (full width at half height 0.075 eV) and the SAPt6Rc basis set. Excitation energies are on the left and oscillator strengths are on the right of state symmetry symbols.

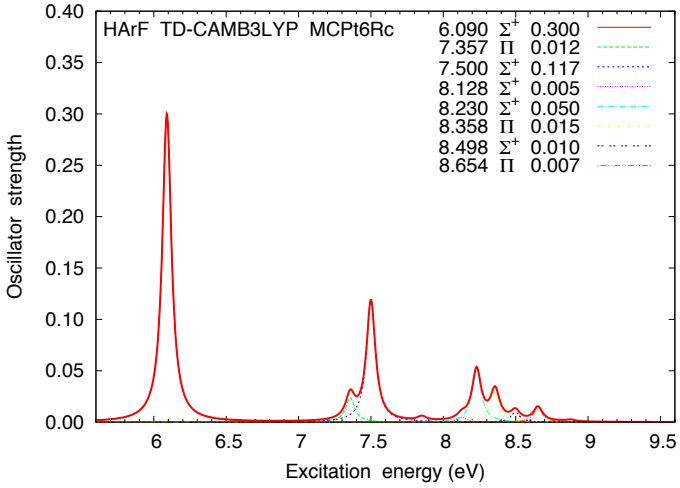

Figure 3.10: HArF singlet absorption spectrum simulated with Cauchy-Lorentz functions (full width at half height 0.075 eV) and the MCPt6Rc basis set. Excitation energies are on the left and oscillator strengths are on the right of state symmetry symbols.

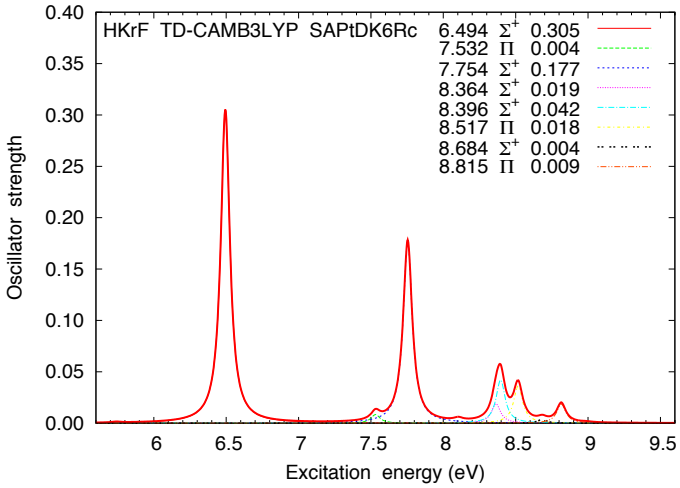

Figure 3.11: HKrF singlet absorption spectrum simulated with Cauchy-Lorentz functions (full width at half height 0.075 eV) and the SAPt6Rc basis set. Excitation energies are on the left and oscillator strengths are on the right of state symmetry symbols.

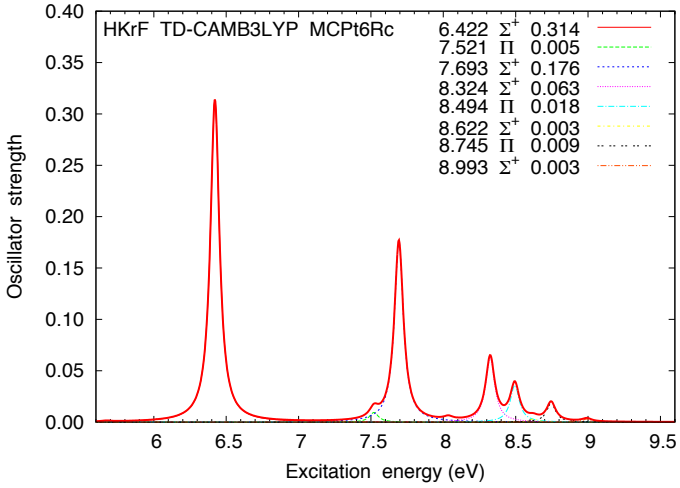

Figure 3.12: HKrF singlet absorption spectrum simulated with Cauchy-Lorentz functions (full width at half height 0.075 eV) and the MCPt6Rc basis set. Excitation energies are on the left and oscillator strengths are on the right of state symmetry symbols.

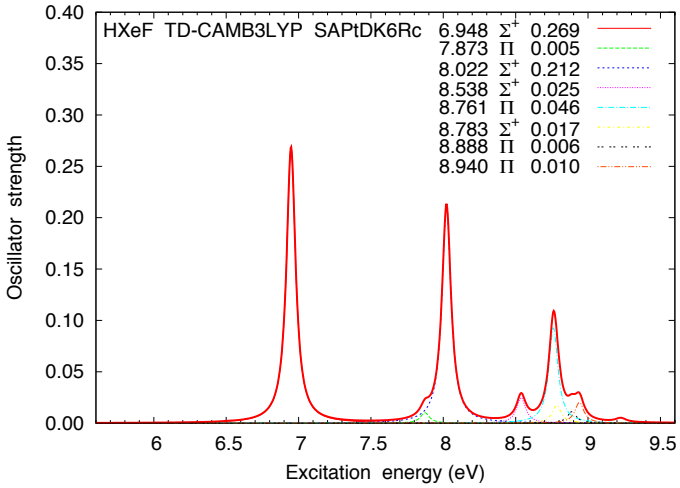

Figure 3.13: HXeF singlet absorption spectrum simulated with Cauchy-Lorentz functions (full width at half height 0.075 eV) and the SAPt6Rc basis set. Excitation energies are on the left and oscillator strengths are on the right of state symmetry symbols.

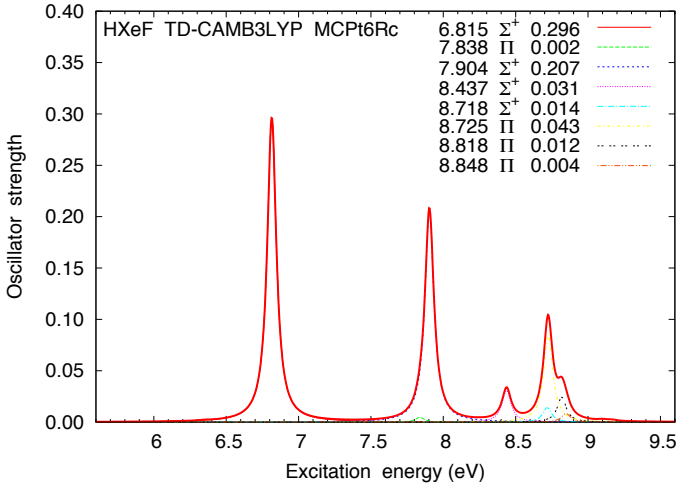

Figure 3.14: HXeF singlet absorption spectrum simulated with Cauchy-Lorentz functions (full width at half height 0.075 eV) and the MCPt6Rc basis set. Excitation energies are on the left and oscillator strengths are on the right of state symmetry symbols.

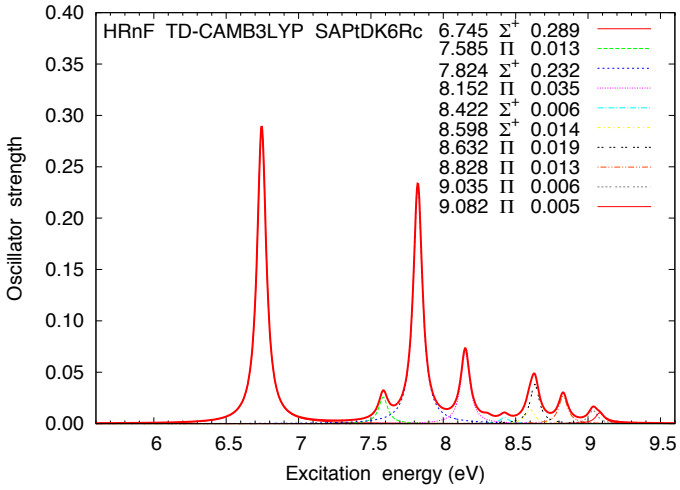

Figure 3.15: HRnF singlet absorption spectrum simulated with Cauchy-Lorentz functions (full width at half height 0.075 eV) and the SAPt6Rc basis set. Excitation energies are on the left and oscillator strengths are on the right of state symmetry symbols.

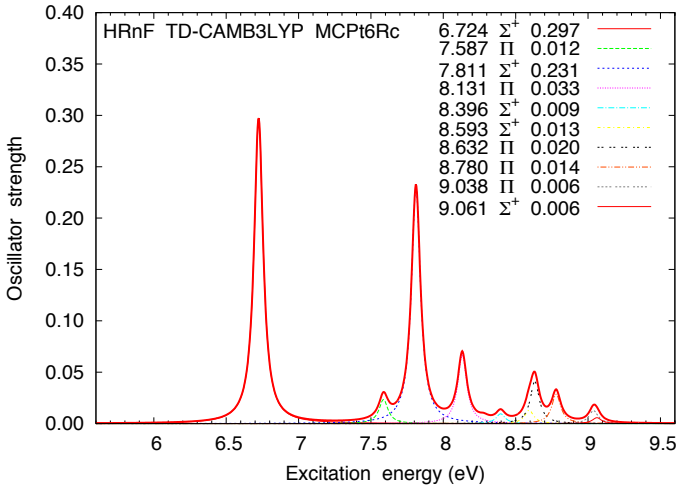

Figure 3.16: HRnF singlet absorption spectrum simulated with Cauchy-Lorentz functions (full width at half height 0.075 eV) and the MCPt6Rc basis set. Excitation energies are on the left and oscillator strengths are on the right of state symmetry symbols.

Table 3.3: Excitation energies (ΔE, in eV) and oscillator strengths (f) for singlet states at TDDFT(CAMB3LYP)/SAPtDK6Rc level of theory [a,b]

HArF			HKrF			HXeF			HRnF		
State	ΔE	f	State	ΔE	f	State	ΔE	f	State	ΔE	f
$1\,^1\Sigma^+$	6.10	0.299	$1\,^1\Sigma^+$	6.49	0.305	$1\,^1\Sigma^+$	6.95	0.269	$1\,^1\Sigma^+$	6.75	0.289
$1\,^1\Pi$	7.34	0.024	$1\,^1\Pi$	7.53	0.008	$1\,^1\Pi$	7.87	0.010	$1\,^1\Pi$	7.59	0.026
$2\,^1\Sigma^+$	7.51	0.121	$2\,^1\Sigma^+$	7.75	0.177	$2\,^1\Sigma^+$	8.02	0.212	$2\,^1\Sigma^+$	7.82	0.232
$3\,^1\Sigma^+$	8.10	0.004	$3\,^1\Sigma^+$	8.36	0.019	$3\,^1\Sigma^+$	8.54	0.025	$2\,^1\Pi$	8.15	0.070
$4\,^1\Sigma^+$	8.22	0.054	$4\,^1\Sigma^+$	8.40	0.042	$2\,^1\Pi$	8.76	0.092	$3\,^1\Sigma^+$	8.42	0.006
$2\,^1\Pi$	8.33	0.030	$2\,^1\Pi$	8.52	0.036	$4\,^1\Sigma^+$	8.78	0.017	$4\,^1\Sigma^+$	8.60	0.014
$5\,^1\Sigma^+$	8.48	0.009	$5\,^1\Sigma^+$	8.68	0.004	$3\,^1\Pi$	8.89	0.012	$3\,^1\Pi$	8.63	0.038
$3\,^1\Pi$	8.64	0.014	$3\,^1\Pi$	8.82	0.018	$4\,^1\Pi$	8.94	0.020	$4\,^1\Pi$	8.83	0.026
									$5\,^1\Pi$	9.03	0.012
									$6\,^1\Pi$	9.08	0.010

[a] Only states with oscillator strengths $f \geq 0.004$ are shown.
[b] Non-relativistic basis set SAPt6Rc was used for HArF.

The electric dipole transitions from the ground state $X\,^1\Sigma^+$ to the $^1\Sigma^-$ and $^1\Delta$ states are forbidden. We will only discuss those $^1\Sigma^+$ and $^1\Pi$ excited states that have large contributions (oscillator strengths) to the peaks in the electronic spectrum. Excitation energies and oscillator strengths of major VUV transitions, calculated using the Sapporo all-electron basis set, are shown in table 3.3 and in figures 3.9, 3.11, 3.13, and 3.15. Major contributions to the excited states and their amplitudes are collected in tables 3.4 – 3.7.

Table 3.4: TDDFT(CAMB3LYP) amplitudes for HArF: basis set SAPt6Rc [(a)]

State	E/eV	f	Major Contributions	Amplitude	Symmetry	Weight
1-Sg	6.10	0.299	1 14 (H) --> 15 (L)	0.958	a1 --> a1	91.9
			2 14 (H) --> 55 (L + 40)	-0.135	a1 --> a1	1.8
1-Pi	7.34	0.012	1 13 (H -1) --> 46 (L + 31)	0.616	b1 --> a1	37.9
			2 13 (H -1) --> 37 (L + 22)	-0.456	b1 --> a1	20.8
2-Sg	7.51	0.121	1 14 (H) --> 46 (L + 31)	0.578	a1 --> a1	33.4
			2 14 (H) --> 37 (L + 22)	-0.452	a1 --> a1	20.4
3-Sg	8.10	0.004	1 13 (H -1) --> 39 (L + 24)	0.393	b1 --> b1	15.4
			2 12 (H -2) --> 38 (L + 23)	0.393	b2 --> b2	15.4
4-Sg	8.22	0.054	1 14 (H) --> 45 (L + 30)	0.498	a1 --> a1	24.8
			2 14 (H) --> 54 (L + 39)	0.403	a1 --> a1	16.3
2-Pi	8.33	0.015	1 13 (H -1) --> 45 (L + 30)	0.555	b1 --> a1	30.8
			2 13 (H -1) --> 54 (L + 39)	0.530	b1 --> a1	28.1
5-Sg	8.48	0.009	1 14 (H) --> 16 (L + 1)	0.449	a1 --> a1	20.1
			2 14 (H) --> 46 (L + 31)	-0.395	a1 --> a1	15.6
3-Pi	8.64	0.007	1 14 (H) --> 44 (L + 29)	0.599	a1 --> b1	35.9
			2 14 (H) --> 53 (L + 38)	0.462	a1 --> b1	21.3

[(a)] HOMO = H = 14, LUMO = L = 15; `N-Sg` and `N-Pi` stand for the N^{th} singlet states of Σ^+ and Π symmetry, respectively; `Symmetry` refers to MO symmetry labels in C_{2v} point group.

Table 3.5: TDDFT(CAMB3LYP) amplitudes for HKrF: basis set SAPtDK6Rc [(a)]

State	E/eV	f	Major Contributions	Amplitude	Symmetry	Weight
1-Sg	6.49	0.305	1 23 (H) --> 24 (L)	0.942	a1 --> a1	88.7
			2 23 (H) --> 55 (L + 31)	0.159	a1 --> a1	2.5
1-Pi	7.53	0.004	1 22 (H -1) --> 55 (L + 31)	0.565	b1 --> a1	32.0
			2 22 (H -1) --> 46 (L + 22)	0.479	b1 --> a1	22.9
2-Sg	7.75	0.177	1 23 (H) --> 55 (L + 31)	0.513	a1 --> a1	26.3
			2 23 (H) --> 46 (L + 22)	0.468	a1 --> a1	21.9
3-Sg	8.36	0.019	1 22 (H -1) --> 48 (L + 24)	0.415	b1 --> b1	17.2
			2 21 (H -2) --> 47 (L + 23)	0.415	b2 --> b2	17.2
4-Sg	8.40	0.042	1 23 (H) --> 54 (L + 30)	0.427	a1 --> a1	18.3
			2 23 (H) --> 49 (L + 25)	0.363	a1 --> a1	13.2
2-Pi	8.52	0.018	1 22 (H -1) --> 54 (L + 30)	0.516	b1 --> a1	26.6
			2 22 (H -1) --> 63 (L + 39)	-0.458	b1 --> a1	20.9
5-Sg	8.68	0.004	1 23 (H) --> 54 (L + 30)	0.460	a1 --> a1	21.2
			2 23 (H) --> 25 (L + 1)	0.442	a1 --> a1	19.6
3-Pi	8.82	0.009	1 23 (H) --> 53 (L + 29)	0.651	a1 --> b1	42.3
			2 23 (H) --> 62 (L + 38)	0.516	a1 --> b1	26.6

[(a)] HOMO = H = 23, LUMO = L = 24; `N-Sg` and `N-Pi` stand for the N^{th} singlet states of Σ^+ and Π symmetry, respectively; `Symmetry` refers to MO symmetry labels in C_{2v} point group.

Table 3.6: TDDFT(CAMB3LYP) amplitudes for HXeF: basis set SAPtDK6Rc [(a)]

State	E/eV	f	Major Contributions	Amplitude	Symmetry	Weight
1-Sg	6.95	0.269	1 32 (H) --> 33 (L)	0.932	a1 --> a1	86.9
			2 32 (H) --> 67 (L + 34)	0.186	a1 --> a1	3.5
1-Pi	7.87	0.005	1 31 (H -1) --> 58 (L + 25)	0.559	b1 --> a1	31.3
			2 31 (H -1) --> 49 (L + 16)	-0.454	b1 --> a1	20.6
2-Sg	8.02	0.212	1 32 (H) --> 58 (L + 25)	0.591	a1 --> a1	34.9
			2 32 (H) --> 49 (L + 16)	-0.537	a1 --> a1	28.8
3-Sg	8.54	0.025	1 32 (H) --> 57 (L + 24)	0.571	a1 --> a1	32.6
			2 32 (H) --> 66 (L + 33)	-0.528	a1 --> a1	27.9
2-Pi	8.76	0.046	1 29 (H -3) --> 33 (L)	0.544	b1 --> a1	29.6
			2 31 (H -1) --> 66 (L + 33)	-0.470	b1 --> a1	22.1
4-Sg	8.78	0.017	1 31 (H -1) --> 56 (L + 23)	0.439	b1 --> b1	19.3
			2 30 (H -2) --> 55 (L + 22)	0.439	b2 --> b2	19.3
3-Pi	8.89	0.006	1 29 (H -3) --> 33 (L)	0.552	b1 --> a1	30.5
			2 31 (H -1) --> 57 (L + 24)	-0.284	b1 --> a1	8.1
4-Pi	8.94	0.010	1 32 (H) --> 62 (L + 29)	0.545	a1 --> b1	29.7
			2 32 (H) --> 71 (L + 38)	0.485	a1 --> b1	23.5

[(a)] HOMO = H = 32, LUMO = L = 33; `N-Sg` and `N-Pi` stand for the N^{th} singlet states of Σ^+ and Π symmetry, respectively; `Symmetry` refers to MO symmetry labels in C_{2v} point group.

Table 3.7: TDDFT(CAMB3LYP) amplitudes for HRnF: basis set SAPtDK6Rc [(a)]

State	E/eV	f	Major Contributions	Amplitude	Symmetry	Weight
1-Sg	6.75	0.289	1 48 (H) --> 49 (L)	0.931	a1 --> a1	86.6
			2 48 (H) --> 74 (L + 25)	0.148	a1 --> a1	2.2
1-Pi	7.59	0.013	1 47 (H -1) --> 71 (L + 22)	0.460	b1 --> a1	21.2
			2 47 (H -1) --> 70 (L + 21)	-0.360	b1 --> a1	13.0
2-Sg	7.82	0.232	1 48 (H) --> 71 (L + 22)	0.478	a1 --> a1	22.9
			2 48 (H) --> 70 (L + 21)	-0.390	a1 --> a1	15.2
2-Pi	8.15	0.035	1 45 (H -3) --> 49 (L)	0.868	b1 --> a1	75.4
			2 45 (H -3) --> 71 (L + 22)	0.247	b1 --> a1	6.1
3-Sg	8.42	0.006	1 48 (H) --> 74 (L + 25)	0.553	a1 --> a1	30.6
			2 48 (H) --> 83 (L + 34)	0.544	a1 --> a1	29.6
4-Sg	8.60	0.014	1 47 (H -1) --> 73 (L + 24)	0.438	b1 --> b1	19.2
			2 46 (H -2) --> 72 (L + 23)	0.438	b2 --> b2	19.2
3-Pi	8.63	0.019	1 47 (H -1) --> 83 (L + 34)	0.510	b1 --> a1	26.1
			2 47 (H -1) --> 74 (L + 25)	0.488	b1 --> a1	23.8
4-Pi	8.83	0.013	1 48 (H) --> 79 (L + 30)	0.613	a1 --> b1	37.6
			2 48 (H) --> 87 (L + 38)	0.603	a1 --> b1	36.4
5-Pi	9.03	0.006	1 47 (H -1) --> 84 (L + 35)	0.436	b1 --> a2	19.0
			2 47 (H -1) --> 76 (L + 27)	-0.427	b1 --> a2	18.3
6-Pi	9.08	0.005	1 47 (H -1) --> 75 (L + 26)	0.519	b1 --> a1	26.9
			2 47 (H -1) --> 62 (L + 13)	0.426	b1 --> a1	18.1

[(a)] HOMO = H = 48, LUMO = L = 49; `N-Sg` and `N-Pi` stand for the N^{th} singlet states of Σ^+ and Π symmetry, respectively; `Symmetry` refers to MO symmetry labels in C_{2v} point group.

To assist in conversion between irreducible representations in the $C_{\infty v}$ point group of the HRgF molecules and the C_{2v} point group used in calculations, corresponding correlations are shown in table 3.8.

Table 3.8: Irreducible representation correlation table

$C_{\infty v}$	C_{2v}	C_{2v} irrep	transformation	
Σ^+	A_1	A_1	z	x^2, y^2, z^2
Σ^-	A_2	A_2		xy
Π	$B_1 + B_2$	B_1	x	xz
Δ	$A_1 + A_2$	B_2	y	yz

The VUV spectrum of each of the four congeners consist of three bands. The lowest energy peak lies between 6.10 and 6.95 eV, with the oscillator strength of $f \approx 0.3$ for all HRgF molecules, and is due to the excitation $X\,^1\Sigma^+ \rightarrow 1\,^1\Sigma^+$. This excitation is predominantly a HOMO-LUMO transition, with both HOMO and LUMO atomic orbitals (AOs) possessing σ^+ symmetry; figure 3.17 illustrates the corresponding orbital shapes for HArF. The HOMO consists mostly of s-type AOs on H and p_z-type AOs on F. The LUMO mainly consists of a somewhat diffuse s-type AO on H and some contributions from p_z-type AOs on Rg and F. Figure 3.17 shows that the electron density around F decreases and the electron density around H increases when going from HOMO to LUMO.

The middle band between 7.34 and 8.02 eV originates mainly in transitions to two states: the dominant $2\,^1\Sigma^+$ and a much-less intense $1\,^1\Pi$ state. Most of the transitions that make up the second $^1\Sigma^+$ excited state are transitions from the HOMO to MOs that have very diffuse character positioned on the Rg (*i.e.* Rydberg orbitals). The $1\,^1\Pi$ state is reached by a transition from an occupied MO composed mainly of a p-type (p_x or p_y) on F to a Rydberg s-type orbital on Rg.

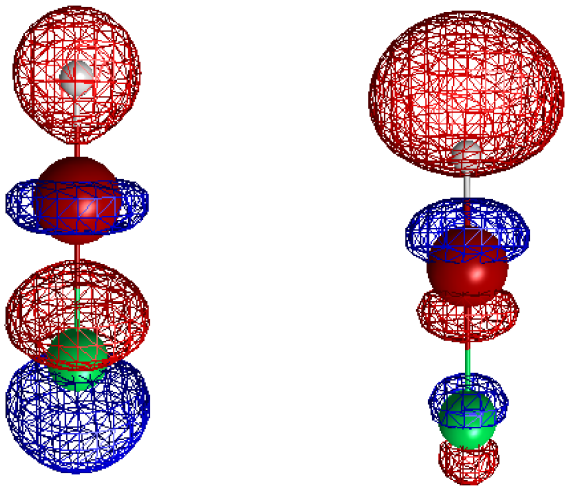

Figure 3.17: Frontier molecular orbitals of HArF: HOMO (left) and LUMO (right).

The highest energy band covers the range above 8.1 eV up to 9.1 eV and consists of two subsystems: the first comprising transitions to two $^1\Sigma^+$ and one $^1\Pi$ state, followed by a group of several states with higher energies. The ordering of the first three states is identical in the first two congeners. For HXeF, the $2\,^1\Pi$ state moves to lower energies with an increased oscillator strength, and for HRnF $2\,^1\Pi$ becomes the lowest-energy, most-intense state in the third spectral band.

Data in tables 3.4 and 3.5 show that for HArF and HKrF the nature of the first three excitations in this band is almost identical, as they originate in electron excitations between the same type of occupied and virtual MOs. Using an abbreviated notation for the MO symmetry, the three states $3\,^1\Sigma^+$, $4\,^1\Sigma^+$, and $2\,^1\Pi$ correspond to $\pi \rightarrow \pi^*$, $\sigma \rightarrow \sigma^*$, and $\pi \rightarrow \sigma^*$ excitations, respectively. However, as revealed in tables 3.6 and 3.7, in the two heavier congeners the lower $^1\Sigma^+$ state is caused by the $\sigma \rightarrow \sigma^*$ excitation while the higher one is due to $\pi \rightarrow \pi^*$ excitation.

The nature of the high-energy part of the third band varies with each congener, with the $^1\Sigma^+$ state being gradually replaced by lower-energy $^1\Pi$ states with larger oscillator strengths.

3.3.2 Effectiveness of the model core potentials

Replacement of core electrons by a pseudopotential results in significantly shorter computing times, visible even for the small systems studied here (table 3.9).

Table 3.9: CPU times (minutes) for TDDFT with either MCPt6Rc or SAPtDK6Rc. The calculations were run using one processor on a 3 GHz MacPro.

system	MCPt6Rc	SAPtDK6Rc
HKrF	77.7	195.6
HXeF	86.1	256.5
HRnF	91.5	344.8

The four HRgF congeners with a progressively heavier central atom allow for a study of effectiveness of the model core potentials. Excitation energies computed with the MCP basis sets are collected in table 3.10. As already shown in figure 3.8, the MCP results have the ability to mimic rather well the all-electron results. A better qualitative insight may be gained by comparing details in figures 3.9 – 3.16 which show that the overall appearance of the VUV spectra is rather similar between the two families of basis sets. A more quantitative insight may be gained by comparing data in tables 3.4 – 3.7 with the corresponding tables 3.11 – 3.14.

Table 3.10: Excitation energies (ΔE, in eV) and oscillator strengths (f) for singlet states at TDDFT(CAMB3LYP)/MCPt6Rc level of theory [a,b]

HArF			HKrF			HXeF			HRnF		
State	ΔE	f	State	ΔE	f	State	ΔE	f	State	ΔE	f
$1\,^1\Sigma^+$	6.09	0.300	$1\,^1\Sigma^+$	6.42	0.314	$1\,^1\Sigma^+$	6.81	0.296	$1\,^1\Sigma^+$	6.72	0.297
$1\,^1\Pi$	7.36	0.024	$1\,^1\Pi$	7.52	0.010	$1\,^1\Pi$	7.84	0.004	$1\,^1\Pi$	7.59	0.024
$2\,^1\Sigma^+$	7.50	0.117	$2\,^1\Sigma^+$	7.69	0.176	$2\,^1\Sigma^+$	7.90	0.207	$2\,^1\Sigma^+$	7.81	0.231
$3\,^1\Sigma^+$	8.13	0.005	$3\,^1\Sigma^+$	8.32	0.063	$3\,^1\Sigma^+$	8.44	0.031	$2\,^1\Pi$	8.13	0.066
$4\,^1\Sigma^+$	8.23	0.050	$2\,^1\Pi$	8.49	0.036	$4\,^1\Sigma^+$	8.72	0.014	$3\,^1\Sigma^+$	8.40	0.010
$2\,^1\Pi$	8.36	0.030	$4\,^1\Sigma^+$	8.62	0.003	$2\,^1\Pi$	8.73	0.086	$4\,^1\Sigma^+$	8.59	0.013
$5\,^1\Sigma^+$	8.50	0.010	$3\,^1\Pi$	8.75	0.018	$3\,^1\Pi$	8.82	0.024	$3\,^1\Pi$	8.63	0.040
$3\,^1\Pi$	8.65	0.014	$5\,^1\Sigma^+$	8.99	0.003	$4\,^1\Pi$	8.85	0.008	$4\,^1\Pi$	8.78	0.028
									$5\,^1\Pi$	9.04	0.012
									$5\,^1\Sigma^+$	9.06	0.006

[a] Only states with oscillator strengths $f \geq 0.003$ are shown.

[b] Non-relativistic MCPs were used used for F and Ar.

Table 3.11: TDDFT(CAMB3LYP) amplitudes for HArF: basis set MCPt6Rc [(a)]

State	E/eV	f	Major Contributions	Amplitude	Symmetry	Weight
1-Sg	6.09	0.300	1 8 (H) --> 9 (L)	0.959	a1 --> a1	91.9
	[-.01]		2 8 (H) --> 49 (L + 40)	-0.129	a1 --> a1	1.7
1-Pi	7.36	0.012	1 7 (H -1) --> 40 (L + 31)	0.620	b1 --> a1	38.5
	[+.02]		2 7 (H -1) --> 31 (L + 22)	0.449	b1 --> a1	20.1
2-Sg	7.50	0.117	1 8 (H) --> 40 (L + 31)	0.588	a1 --> a1	34.5
	[-.01]		2 8 (H) --> 31 (L + 22)	0.447	a1 --> a1	20.0
3-Sg	8.13	0.005	1 7 (H -1) --> 33 (L + 24)	0.393	b1 --> b1	15.5
	[+.03]		2 6 (H -2) --> 32 (L + 23)	0.393	b2 --> b2	15.5
4-Sg	8.23	0.050	1 8 (H) --> 39 (L + 30)	0.494	a1 --> a1	24.4
	[+.01]		2 8 (H) --> 48 (L + 39)	-0.402	a1 --> a1	16.2
2-Pi	8.36	0.015	1 7 (H -1) --> 39 (L + 30)	0.558	b1 --> a1	31.1
	[+.03]		2 7 (H -1) --> 48 (L + 39)	-0.531	b1 --> a1	28.1
5-Sg	8.50	0.010	1 8 (H) --> 10 (L + 1)	0.443	a1 --> a1	19.6
	[+.02]		2 8 (H) --> 40 (L + 31)	0.395	a1 --> a1	15.6
3-Pi	8.65	0.007	1 8 (H) --> 38 (L + 29)	0.601	a1 --> b1	36.1
	[+.01]		2 8 (H) --> 47 (L + 38)	-0.459	a1 --> b1	21.0

[(a)] HOMO = H = 8, LUMO = L = 9; `N-Sg` and `N-Pi` stand for the N^{th} singlet states of Σ^+ and Π symmetry, respectively; `Symmetry` refers to MO symmetry labels in C_{2v} point group. The values in square brackets are deviations from the SAPtDK6Rc values: [X] = E(MCPt6Rc) - E(SAPtDK6Rc).

Table 3.12: TDDFT(CAMB3LYP) amplitudes for HKrF: basis set MCPt6Rc [(a)]

State	E/eV	f	Major Contributions	Amplitude	Symmetry	Weight
1-Sg	6.42	0.314	1 13 (H) --> 14 (L)	0.942	a1 --> a1	88.8
	[-.05]		2 13 (H) --> 45 (L + 31)	-0.157	a1 --> a1	2.5
1-Pi	7.52	0.005	1 12 (H -1) --> 45 (L + 31)	0.565	b1 --> a1	31.9
	[-.01]		2 12 (H -1) --> 36 (L + 22)	0.482	b1 --> a1	23.2
2-Sg	7.69	0.176	1 13 (H) --> 45 (L + 31)	0.513	a1 --> a1	26.3
	[-.06]		2 13 (H) --> 36 (L + 22)	0.472	a1 --> a1	22.3
3-Sg	8.32	0.063	1 13 (H) --> 44 (L + 30)	0.439	a1 --> a1	19.2
	[-.04]		2 13 (H) --> 39 (L + 25)	-0.384	a1 --> a1	14.7
2-Pi	8.49	0.018	1 12 (H -1) --> 44 (L + 30)	0.517	b1 --> a1	26.7
	[-.03]		2 12 (H -1) --> 53 (L + 39)	-0.450	b1 --> a1	20.2
4-Sg	8.62	0.003	1 13 (H) --> 44 (L + 30)	0.453	a1 --> a1	20.5
	[+.22]		2 13 (H) --> 15 (L + 1)	0.436	a1 --> a1	19.0
3-Pi	8.75	0.009	1 13 (H) --> 43 (L + 29)	0.646	a1 --> b1	41.7
	[-.07]		2 13 (H) --> 52 (L + 38)	-0.517	a1 --> b1	26.7
5-Sg	8.99	0.003	1 13 (H) --> 15 (L + 1)	0.514	a1 --> a1	26.4
	[+.31]		2 13 (H) --> 35 (L + 21)	-0.368	a1 --> a1	13.5

[(a)] HOMO = H = 13, LUMO = L = 14; `N-Sg` and `N-Pi` stand for the N^{th} singlet states of Σ^+ and Π symmetry, respectively; `Symmetry` refers to MO symmetry labels in C_{2v} point group. The values in square brackets are deviations from the SAPtDK6Rc values: [X] = E(MCPt6Rc) - E(SAPtDK6Rc).

Table 3.13: TDDFT(CAMB3LYP) amplitudes for HXeF: basis set MCPt6Rc [(a)]

State	E/eV	f	Major Contributions	Amplitude	Symmetry	Weight
1-Sg	6.81	0.296	1 13 (H) --> 14 (L)	0.937	a1 --> a1	87.8
	[-.14]		2 13 (H) --> 48 (L + 34)	0.179	a1 --> a1	3.2
1-Pi	7.84	0.002	1 12 (H -1) --> 39 (L + 25)	0.544	b1 --> a1	29.6
	[-.03]		2 12 (H -1) --> 30 (L + 16)	0.468	b1 --> a1	21.9
2-Sg	7.90	0.207	1 13 (H) --> 39 (L + 25)	0.568	a1 --> a1	32.3
	[-.12]		2 13 (H) --> 30 (L + 16)	0.537	a1 --> a1	28.8
3-Sg	8.44	0.031	1 13 (H) --> 38 (L + 24)	0.553	a1 --> a1	30.6
	[-.10]		2 13 (H) --> 47 (L + 33)	-0.519	a1 --> a1	26.9
4-Sg	8.72	0.014	1 11 (H -2) --> 36 (L + 22)	0.429	b2 --> b2	18.4
	[-.06]		2 12 (H -1) --> 37 (L + 23)	-0.429	b1 --> b1	18.4
2-Pi	8.73	0.043	1 10 (H -3) --> 14 (L)	0.555	b1 --> a1	30.8
	[-.03]		2 12 (H -1) --> 47 (L + 33)	-0.462	b1 --> a1	21.3
3-Pi	8.82	0.012	1 13 (H) --> 43 (L + 29)	0.501	a1 --> b1	25.1
	[-.07]		2 13 (H) --> 52 (L + 38)	0.454	a1 --> b1	20.6
4-Pi	8.85	0.004	1 10 (H -3) --> 14 (L)	0.535	b1 --> a1	28.6
	[-.09]		2 13 (H) --> 43 (L + 29)	-0.358	a1 --> b1	12.8

[(a)] HOMO = H = 13, LUMO = L = 14; `N-Sg` and `N-Pi` stand for the N^{th} singlet states of Σ^+ and Π symmetry, respectively; `Symmetry` refers to MO symmetry labels in C_{2v} point group. The values in square brackets are deviations from the SAPtDK6Rc values: [X] = E(MCPt6Rc) - E(SAPtDK6Rc).

Table 3.14: TDDFT(CAMB3LYP) amplitudes for HRnF: basis set MCPt6Rc [(a)]

State	E/eV	f	Major Contributions			Amplitude	Symmetry		Weight
1-Sg	6.72	0.297	1	13 (H) -->	14 (L)	0.932	a1 -->	a1	86.8
	[-.03]		2	13 (H) -->	39 (L + 25)	0.146	a1 -->	a1	2.1
1-Pi	7.59	0.012	1	12 (H -1) -->	36 (L + 22)	0.491	b1 -->	a1	24.1
	[0.00]		2	12 (H -1) -->	42 (L + 28)	0.367	b1 -->	a1	13.5
2-Sg	7.81	0.231	1	13 (H) -->	36 (L + 22)	0.507	a1 -->	a1	25.7
	[-.01]		2	13 (H) -->	42 (L + 28)	0.359	a1 -->	a1	12.9
2-Pi	8.13	0.033	1	10 (H -3) -->	14 (L)	0.875	b1 -->	a1	76.6
	[-.02]		2	10 (H -3) -->	36 (L + 22)	0.253	b1 -->	a1	6.4
3-Sg	8.40	0.010	1	13 (H) -->	39 (L + 25)	0.561	a1 -->	a1	31.4
	[-.04]		2	13 (H) -->	48 (L + 34)	0.522	a1 -->	a1	27.2
4-Sg	8.59	0.013	1	11 (H -2) -->	37 (L + 23)	0.431	b2 -->	b2	18.6
	[-.01]		2	12 (H -1) -->	38 (L + 24)	-0.431	b1 -->	b1	18.6
3-Pi	8.63	0.020	1	12 (H -1) -->	48 (L + 34)	0.505	b1 -->	a1	25.5
	[0.00]		2	12 (H -1) -->	39 (L + 25)	0.491	b1 -->	a1	24.1
4-Pi	8.78	0.014	1	13 (H) -->	44 (L + 30)	0.628	a1 -->	b1	39.4
	[-.05]		2	13 (H) -->	52 (L + 38)	0.606	a1 -->	b1	36.8
5-Pi	9.04	0.006	1	12 (H -1) -->	50 (L + 36)	0.437	b1 -->	a2	19.1
	[-.01]		2	12 (H -1) -->	40 (L + 26)	-0.425	b1 -->	a2	18.1
5-Sg	9.06	0.006	1	13 (H) -->	45 (L + 31)	0.489	a1 -->	a1	23.9
			2	13 (H) -->	30 (L + 16)	-0.408	a1 -->	a1	16.6

[(a)] HOMO = H = 13, LUMO = L = 14; `N-Sg` and `N-Pi` stand for the N^{th} singlet states of Σ^+ and Π symmetry, respectively; `Symmetry` refers to MO symmetry labels in C_{2v} point group. The values in square brackets are deviations from the SAPtDK6Rc values: [X] = E(MCPt6Rc) - E(SAPtDK6Rc).

The ability of the MCPs to mimic the results obtained with the all-electron basis set depends on the Rg atom, as already seen in figure 3.8, with the Ar and Rn results being the closest. For HArF, where an MCP replaces only the Ne core, the differences in excitation energies vary between −0.01 eV to +0.03 eV. It is gratifying to see that the structure of both occupied and virtual orbital spaces is identical, as shown by identical orbital excitations in the major contributions and with very similar

amplitudes (tables 3.4 and 3.11).

Agreement is much worse for HKrF, where the Kr electrons explicitly included in calculations are $3d^{10}\,4s^2\,4p^6$ and an MCP replaced the Ar core. The deviations of excitation energies are in the range -0.01 eV to $+0.31$ eV, with the largest errors found for the $^1\Sigma^+$ states; these deviations change the ordering of the highest four excited states. The description of excitations in terms of orbital numbering remains the same only for the four lowest states; for the higher states, only the $^1\Pi$ states are described by identical orbital excitations (tables 3.5 and 3.12).

In comparison with HKrF, the results for HXeF shows an improved agreement between the all-electron and MCP data. The Xe atom has an analogous valence electron configuration as Kr, $4d^{10}\,5s^2\,5p^6$, with the 36 electrons of Kr core replaced by a pseudopotential. The errors in excitation energies are smaller than for HKrF, and range between -0.003 eV and -0.14 eV, with deviations for the $^1\Pi$ states again smaller than for the $^1\Sigma^+$ states, resulting in the interchange of $2\,^1\Pi$ and $4\,^1\Sigma^+$ states. Orbital characterization of the major contributions is the same except for the two highest $^1\Pi$ states (tables 3.6 and 3.13).

Rather surprisingly, the agreement between the AE and MCP results for the heaviest congener is the best, with errors in excitation energies between 0.0 and -0.05 eV (tables 3.7 and 3.14). The valence space for Rn is analogous to that in Kr and Xe, $5d^{10}\,6s^2\,6p^6$, with the remaining 68 electrons (Xe core plus $4f^{14}$ subshell) represented by an MCP. The ordering of the excited states is the same except for the highest, tenth state, which is predicted to be $6\,^1\Pi$ by AE calculations and $5\,^1\Sigma^+$ by the MCP method. Notably, orbital excitations involved in the main contributions to the excited states are identical in both approaches.

3.3.3 Spectra of HRgF in Rg matrices (Rg = Ar, Kr)

Figure 3.18 shows that the HRgF@Rg_{12} spectra are shifted to higher energies relative to the free HRgF. This shift may be due to the interaction between the large charges on the atoms in HRgF with the atoms in the matrix; this is believed to cause the matrix shifts in its vibrational spectra [16]. When comparing the orbital energies, the LUMO of HRgF@Rg_{12} was destabilized relative to free HRgF.

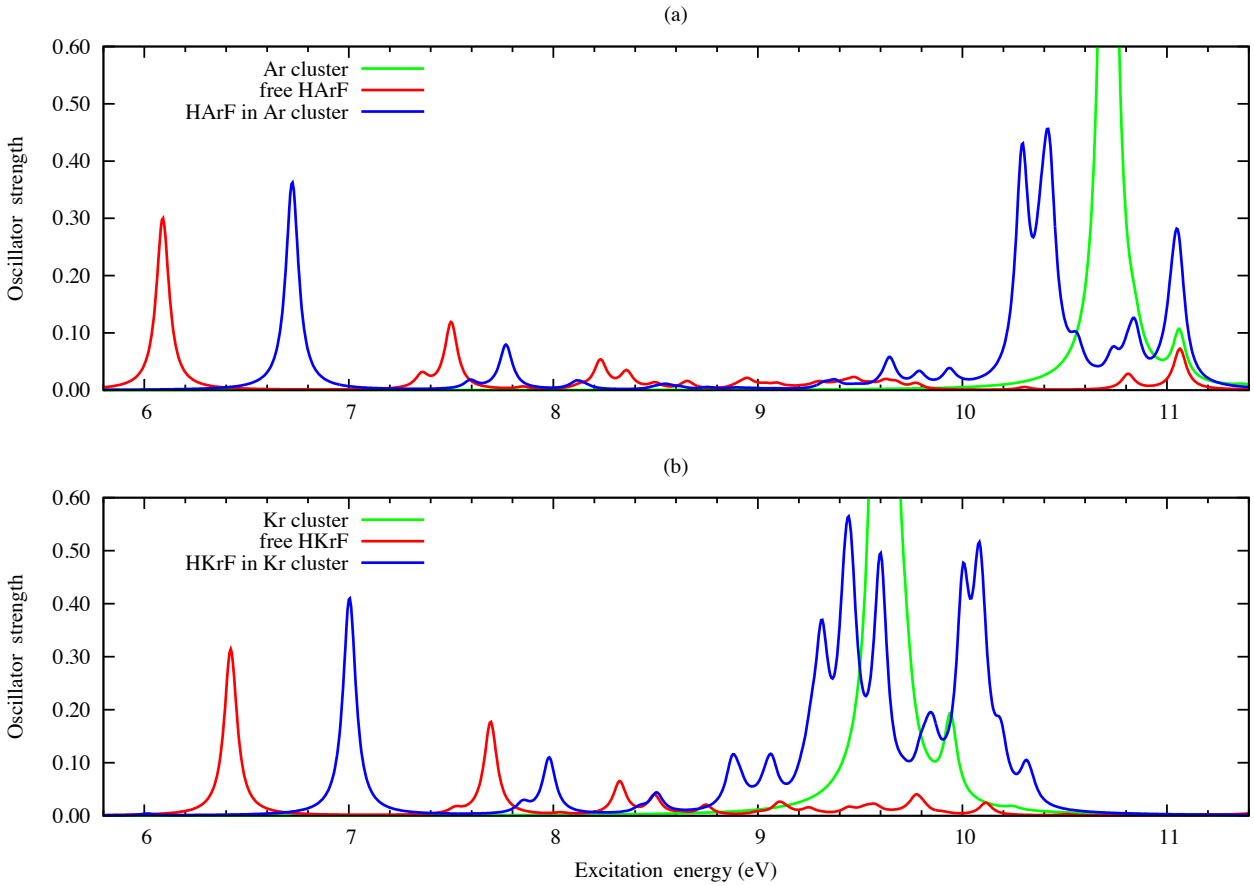

Figure 3.18: Electronic spectra of the HRgF@Rg_{12} (Rg = Ar, Kr) using TDDFT/M-CPt6Rc.

The $HArF@Ar_{12}$ spectrum shows a strong peak near 11 eV while that for $HKrF@Kr_{12}$ contains a strong peak near 9.5 eV. These high energy, strong intensity peaks belong to the Rg matrix as found in calculations for $Rg@Rg_{12}$. The Rg cluster peak does not overlap with the HRgF spectrum region. In $HKrF@Kr_{12}$, the HKrF part of the spectrum was closer to the krypton cluster peak than HArF was to the argon cluster peak; therefore, a good spectral resolution would be required when attempting to identify the VUV spectrum of HKrF experimentally. The HOMO-LUMO peak (6.8 eV for HArF and 7.0 eV for HKrF) would be most useful for identification purposes in an experimental VUV spectrum of HRgF.

To study possible spectral contamination, TDDFT/MCPt calculations on HF, which is a dissociation product of HArF and HKrF, were also performed at the experimental equilibrium distance $r_e = 0.9169$ Å. The electronic spectrum of HF occurs at energies higher than the Rg peak (with the first transition at 10.06 eV, due to excitation to the $^1\Pi$ state), thus HF will likely not contaminate the HRgF spectral region.

Another possible contaminant is the excimer Rg_2F. Hakuta *et al.* experimentally found that in the spectrum of Ar_2F a peak occurs at 248 nm (5.00 eV) which is far away from the spectrum of HArF [76]. Similarly, Ahokas *et al.* found, experimentally, that Xe_2Cl had its spectral peaks away from the HXeCl region of the spectrum [2]. Geohegan *et al.* found that Kr_2F's spectrum is from 248 nm to 570 nm (2.18 eV to 5.00 eV) [77]. The Rg_2F spectrum will likely appear next to the HRgF spectrum in the experimental VUV spectrum for Rg= Ar, Kr.

Other possible contaminants include the caged H atom and RgF. Ahokas *et al.* found that caged H (in Xe matrix) has its peaks at 198 nm and 201 nm (6.26 eV and 6.20 eV, respectively) [2]. It is likely that the peaks of caged H in an Ar or Kr matrix could appear close to the HOMO-LUMO peak of HRgF. Because of all the possible contaminants, a difference spectrum may be required for the experimental spectrum of HRgF.

Bressler *et al.* discussed the electronic spectra of other argon species and krypton species; these rare gas species may appear in HArF and HKrF experimental VUV spectra [78].

3.3.4 Scalar relativistic effects in the HRgF spectra

The scalar relativistic effects in electronic spectra of HArF and HKrF were negligible; therefore, the PolX6Rc (non-relativistic) and PolXDK6Rc (scalar relativistic) results are shown for HXeF and HRnF. Figure 3.19 shows that the main result of relativistic effects is the red shift of the first peak for both HXeF and HRnF; as expected, the shifts are more prominent for HRnF than for HXeF.

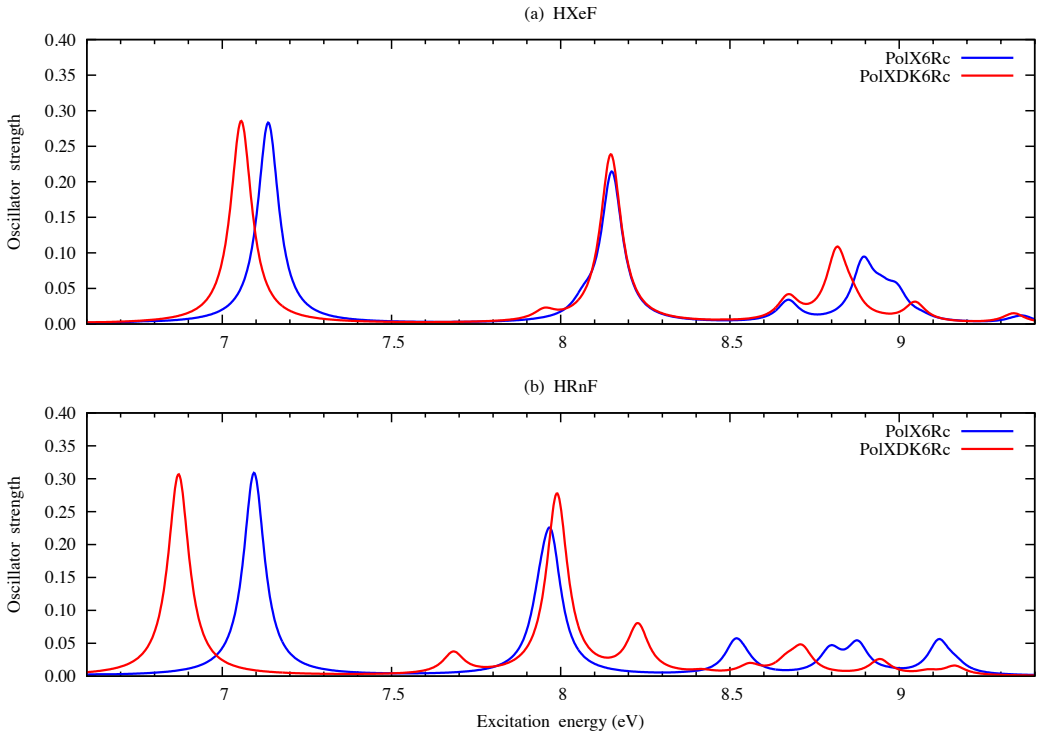

Figure 3.19: Electronic spectra of HXeF and HRnF at the TDDFT/PolX6Rc (non-relativistic) and TDDFT/PolXDK6Rc (scalar relativistic) levels of theory, respectively.

Detailed results for HRnF are collected in tables 3.15 and 3.16. Since the HOMO-LUMO peak shows the greatest red shift due to relativistic effects and is the peak most important for experimental identification, we will focus our analysis on it.

Table 3.15: TDDFT excitation energies (ΔE, in eV) and oscillator strengths (f) for HRnF.

	PolX6Rc		PolXDK6Rc			MCPt6Rc	
state	ΔE	f	ΔE	$\Delta\Delta E^{(a)}$	f	ΔE	f
$1\,^1\Sigma^+$	7.09	0.309	6.87	-0.22	0.306	6.72	0.297
$2\,^1\Sigma^+$	7.97	0.183	7.99	0.02	0.275	7.81	0.231
$3\,^1\Sigma^+$	8.54	0.012	8.56	0.02	0.013	8.40	0.010
$4\,^1\Sigma^+$	8.80	0.031	8.67	-0.13	0.016	8.59	0.013
$1\,^1\Pi$	7.94	0.065	7.68	-0.26	0.032	7.59	0.023
$2\,^1\Pi$	8.37	0.000	8.23	-0.14	0.073	8.13	0.066
$3\,^1\Pi$	8.52	0.046	8.42	-0.10	0.004	8.28	0.003
$4\,^1\Pi$	8.79	0.006	8.71	-0.08	0.038	8.63	0.041
$5\,^1\Pi$	8.88	0.045	8.94	0.06	0.022	8.78	0.029

$^{(a)}$ Effect of relativity on excitation energies, $\Delta\Delta E = \Delta E(\text{PolXDK6Rc}) - \Delta E(\text{PolX6Rc})$.

The shifts in excitation energy are rather small: the HOMO-LUMO peak $1\,^1\Sigma^+$ is red shifted by 0.22 eV; excitation to $1\,^1\Pi$ experiences similar shift of 0.26 eV. Most of the shifts are smaller and range from 0.01 eV to 0.14 eV. Similar minute differences were found by Rosa *et al.* for $W(CO)_6$ [79] and Romaniello *et al.* for $[Pt(H_2timdt)_2]$ [80]. They found more blue shifts instead of red shifts, likely because the valence MOs of these two compounds had more d-character which expand with relativistic effects.

Orbital energy differences between the occupied and virtual orbitals might be used to estimate changes in the excitation energies; the relevant relativistic and non-relativistic valence orbital energies for HRnF are tabulated in table 3.16. The rela-

tivistic basis set has little effect on the stabilization (orbital energy) of HOMO, but it stabilizes (decreases the orbital energy) of the LUMO by 0.20 eV. The energy gap between the HOMO and LUMO is smaller when relativistic effects are included; this may explain why the excitation energy corresponding to the HOMO-LUMO transition ($1\,^1\Sigma^+$) is lower with the relativistic calculations than for the non-relativistic calculations. Rosa *et al.* found that the $3t_{2g}$ and $6e_g$ orbitals of $W(CO)_6$ are both destabilized when relativistic effects are included, due to the $5d$ orbitals on W becoming more diffuse [79]. For HRnF, the HOMO and LUMO become more stabilized because these orbitals are mainly composed of s-type AOs that contract due to relativistic effects, making the energy gap smaller and thus, making the excitation energy smaller.

Table 3.16: Non-relativistic (PolX6Rc) and relativistic (PolXDK6Rc) CAMB3LYP valence orbitals energies for HRnF [(a)]

Symmetry	$\varepsilon_{\text{PolX6Rc}}$	$\varepsilon_{\text{PolXDK6Rc}}$
σ^+ (LUMO)	-0.45	-0.65
σ^+ (HOMO)	-9.91	-9.92
π	-10.29	-10.12
π	-12.28	-12.30
σ^+	-15.18	-15.16
σ^+	-22.75	-27.47
σ^+	-31.07	-31.00
δ	-58.15	-52.40
π	-58.52	-52.74
σ^+	-58.67	-52.90

[(a)] All values in eV.

3.3.5 Spin-orbit effects in the spectra of HXeF and HRnF

The presence of heavy atoms Xe and Rn warrants an investigation of the effects of spin-orbit coupling (SOC) on the electronic spectra. These effects were evaluated using the Amsterdam Density Functional (ADF) program [81, 82], because GAMESS-US lacks the ability to carry out SOC TDDFT calculations. The CAMYB3LYP functional [83] was used, together with an extensive Slater-type quadruple-zeta basis set containing four polarization functions (QZ4P or qz4p) [47]. The QZ4P basis set lacks diffuse functions and thus is not suitable for describing the Rydberg states; therefore only the lowest excited states were studied.

To check whether the two related functionals, CAMYB3LYP and CAMB3LYP, implemented in two programs, ADF and GAMESS-US, and using different basis sets bring about comparable results, the CAMYB3LYP/QZ4P excitation energies and oscillator strengths were evaluated for HXeF and HRnF using the scalar relativistic zeroth-order regular approximation (ZORA) [84–87]. Table 3.17 shows that the results compare quite well with the ones obtained using the DKH2 scalar approximation [72, 73, 88] at the CAMB3LYP/SAPt6Rc level of theory. In both sets of calculations all electrons were explicitly treated.

Table 3.17: Comparison of excitation energies for singlet states at CAMYB3LYP/QZ4P and CAMB3LYP/SAPt6Rc levels of theory [a,b]

	HXeF		HRnF	
State	ΔE	f	ΔE	f
$1\,^1\Sigma^+$	6.95 (6.95)	0.280 (0.269)	6.75 (6.75)	0.277 (0.289)
$1\,^1\Pi$	7.82 (7.87)	0.022 (0.010)	7.45 (7.59)	0.041 (0.026)
$2\,^1\Sigma^+$	8.12 (8.02)	0.286 (0.212)	7.89 (7.82)	0.296 (0.212)
$2\,^1\Pi$			8.05 (8.15)	0.069 (0.070)

[a] Excitation energies ΔE in eV. Only transitions with oscillator strengths $f \geq 0.003$ are shown; contributions from components of degenerate transitions are included. [b] CAMB3LYP/SAPt6Rc values (from table 3.3) are shown in parentheses.

For the lighter system HXeF the SOC effects on the spectra are rather small and manifested by minor red shifts as shown in figure 3.20 and table 3.18.

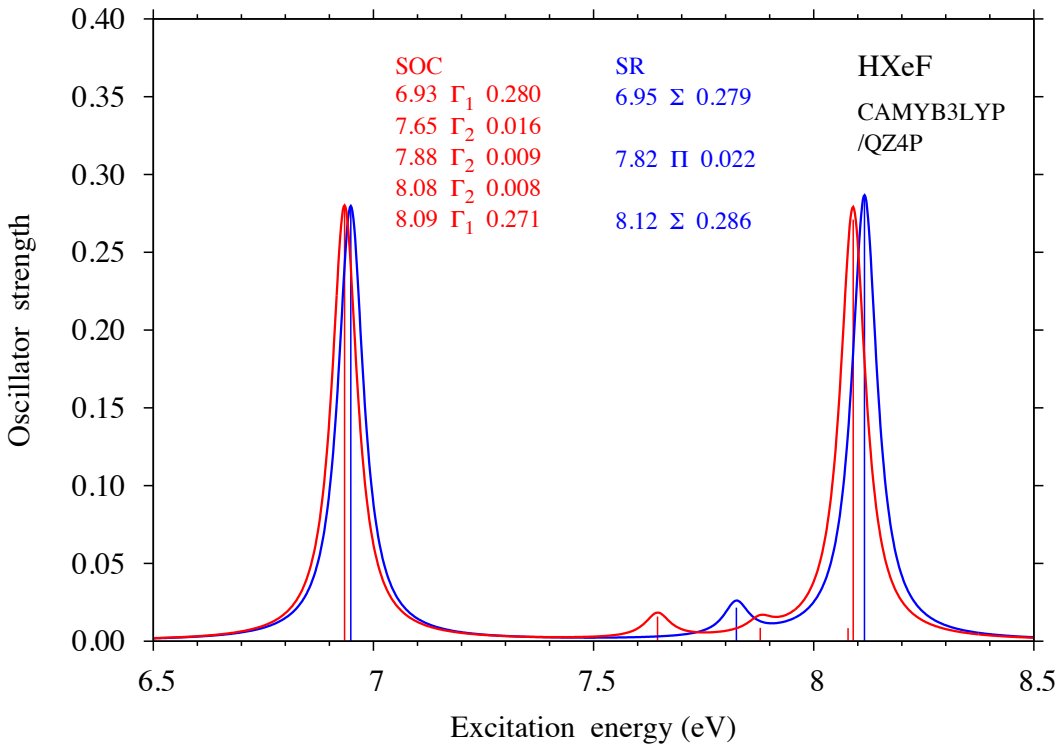

Figure 3.20: Electronic spectra of HXeF with (SOC) and without (SR) spin-orbit coupling. The symbols Σ and Π stand for excitations to $^1\Sigma^+$ and $^1\Pi$ states, respectively, in the scalar relativistic (SR) approximation. The symbols Γ_1 and Γ_2 represent non-degenerate and doubly-degenerate levels in the SOC approximation. Excitation energies are on the left and oscillator strengths are on the right of the state symbols.

Table 3.18: Main low-lying SOC transitions in HXeF and their contributing SR transitions [a]

SOC transition			Scalar relativistic contribution			
State[b]	ΔE	f	Weight[c]	State	ΔE	f
$2\,\Gamma_1$	6.93	0.280	0.93	$1\ ^1\Sigma^+$	6.95	0.280
$5\,\Gamma_2$	7.65	0.016	0.69	$2\ ^3\Pi$	7.73	
			0.30	$2\ ^1\Pi$	7.82	0.022
$6\,\Gamma_2$	7.88	0.009	0.68	$2\ ^1\Pi$	7.82	0.022
			0.30	$2\ ^3\Pi$	7.73	
$7\,\Gamma_2$	8.08	0.008	0.80	$3\ ^3\Pi$	8.22	
			0.17	$3\ ^1\Pi$	8.74	0.049
$4\,\Gamma_1$	8.09	0.271	0.89	$2\ ^1\Sigma^+$	8.12	0.286

[a] Excitation energies ΔE in eV. Only transitions with oscillator strengths $f \geq 0.008$ are shown; contributions from components of degenerate transitions are included. [b] The symbols Γ_1 and Γ_2 represent non-degenerate and doubly-degenerate levels, respectively, in the SOC approximation. [c] Weight denotes the fractional contribution of the scalar relativistic transitions to the SOC transition.

However, for HRnF the spectral changes are more pronounced. The effect of the SOC on excitation energies, as illustrated in figure 3.21, shifts the main SR peaks from 6.75 eV and 7.89 eV by 0.1 eV and 0.15 eV, respectively, towards lower energies. In addition, several new transitions appear, resulting from the coupling between singlet and triplet states and changing the appearance of the spectrum.

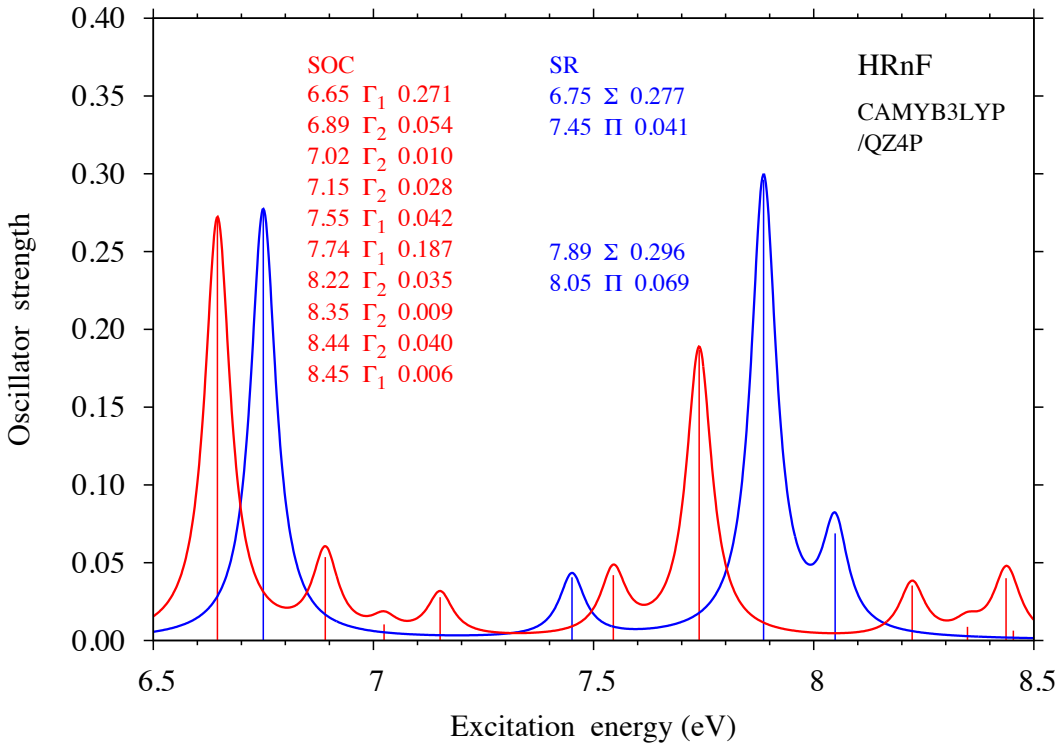

Figure 3.21: Electronic spectra of HRnF with (SOC) and without (SR) spin-orbit coupling. The symbols Σ and Π stand for excitations to $^1\Sigma^+$ and $^1\Pi$ states, respectively, in the scalar relativistic (SR) approximation. The symbols Γ_1 and Γ_2 represent non-degenerate and doubly-degenerate levels in the SOC approximation. Excitation energies are on the left and oscillator strengths are on the right of the state symbols.

Table 3.19: Main low-lying SOC transitions in HRnF and their contributing SR transitions [a]

SOC transition			Scalar relativistic contribution			
State[b]	ΔE	f	Weight[c]	State	ΔE	f
$2\,\Gamma_1$	6.65	0.271	0.90	$1\ ^1\Sigma^+$	6.75	0.277
$4\,\Gamma_2$	6.89	0.054	0.55	$2\ ^3\Pi$	7.32	
			0.33	$2\ ^1\Pi$	7.45	0.041
$5\,\Gamma_2$	7.02	0.010	0.91	$2\ ^3\Sigma^+$	7.15	
			0.07	$2\ ^1\Pi$	7.45	0.041
$6\,\Gamma_2$	7.15	0.028	0.54	$3\ ^3\Pi$	7.52	
			0.30	$3\ ^1\Pi$	8.05	0.069
$3\,\Gamma_1$	7.55	0.042	0.38	$2\ ^3\Pi$	7.32	
			0.38	$2\ ^3\Pi$	7.32	
$4\,\Gamma_1$	7.74	0.187	0.68	$2\ ^1\Sigma^+$	7.89	0.296
			0.05	$2\ ^3\Pi$	7.32	
$8\,\Gamma_2$	8.22	0.035	0.35	$3\ ^1\Pi$	8.05	0.069
			0.30	$6\ ^3\Sigma^+$	9.72	
$9\,\Gamma_2$	8.35	0.009	0.43	$4\ ^3\Sigma^+$	8.94	
			0.34	$1\ ^3\Sigma^-$	9.05	
$10\,\Gamma_2$	8.44	0.040	0.35	$5\ ^3\Pi$	8.86	
			0.20	$5\ ^1\Pi$	9.03	0.150
$5\,\Gamma_1$	8.45	0.006	0.24	$3\ ^3\Pi$	7.52	
			0.24	$3\ ^3\Pi$	7.52	

[a] Excitation energies ΔE in eV. Only transitions with oscillator strengths $f \geq 0.006$ are shown; contributions from components of degenerate transitions are included. [b] The symbols Γ_1 and Γ_2 represent non-degenerate and doubly-degenerate levels, respectively, in the SOC approximation. [c] Weight denotes the fractional contribution of the scalar relativistic transitions to the SOC transition.

The composition of the main SOC excitation energies in the low-energy range for HRnF is shown in table 3.19. The two peaks at 6.89 eV and 7.02 eV result from coupling between the SR singlet Π state (7.45 eV) with different triplet states. The peak at 7.15 eV results from a mixture of singlet and triplet states; its oscillator strength ($f = 0.028$) is about half of that corresponding to the singlet component ($f = 0.069$). The peak at 7.55 eV is mainly a triplet state, transition to which was forbidden in the SR approach. The major contribution to the 7.74 eV peak is the singlet transition at 7.89 eV (68%); accordingly, its oscillator strength is fairly large ($f = 0.187$). The main contribution to the 8.22 eV peak is the third $^1\Pi$ SR transition, the same that contributed to the SOC peak at 7.15 eV; however, an admixture of a $^3\Sigma^+$ state at a high energy (9.72 eV) results in a blue shift of the SR transition. Of the three remaining peaks in the SOC spectrum, the most intense at 8.44 eV contains a contribution from the fifth $^1\Pi$ SR transition.

The variation of the electronic spectrum of HRnF upon the inclusion of spin-orbit coupling indicates the need for simulation of spectra that goes beyond the scalar relativistic approximation. It remains to be seen whether this conclusion remains valid for other compounds containing radon.

3.4 Conclusions

The electronic spectra of the HRgF (Rg= Ar, Kr, Xe, Rn) family were generated at the TDDFT level of theory using all-electron and pseudopotential basis sets and assignment of features in the spectra were carried out. The lowest energy peak has the highest intensity and is primarily due to the HOMO-LUMO transition ($1\,^1\Sigma^+$). The other peaks are mostly due to an electronic transition from HOMO to diffuse MOs. Transitions from an occupied orbital with π character to a Rydberg orbital were also found.

The computed electronic spectrum of HRgF@Rg_{12} (Rg = Ar, Kr) showed a large peak at 11 eV for Ar and 9.5 eV for Kr. This peak corresponds to the Rg matrix

peak and it might interfere with the HRgF peaks.

Performance of the MCP-TZP basis set was compared with that of the all-electron basis set. The MCP-TZP basis set yielded excitation energies that were closer to those obtained with the Sapporo-DKH3-TZP-2012 basis set than to those computed using the PolXDK basis set; this is not surprising, as MCP-TZP and the Sapporo basis sets have very similar set of polarization/correlating functions. The MCP-TZP basis set was also the most efficient of the basis sets used, reducing computing time by a factor of about 2.5 for HKrF to 3.8 for HRnF.

Relativistic effects affect the spectra of the systems that contain the heaviest rare gas atoms, HXeF and HRnF. Scalar relativistic effects are manifested in red shifts in the spectra. The peak that shifts the most due to the scalar relativistic effects is the one that involves the HOMO-LUMO excitation. The orbital energy of HOMO does not significantly change but that of the the LUMO decreases, reducing the energy gap between these MOs. This explains the decrease in excitation energy (red shift) of the HOMO-LUMO peak. The LUMO is mostly composed of s-type and p-type AOs which are expected to contract when relativistic effects are incorporated. This contraction is indeed observed by the indication of the LUMO's orbital energy decreasing (LUMO is stabilized by relativistic effects). A significant effect due to the spin-orbit coupling that combines singlet and triplet excited states is found in HRnF, where a number of new excitations appear, underlying the important role that the spin-orbit coupling plays in the simulations of electronic spectra in systems containing atoms of heavy elements.

Chapter 4

Structure, reactions, and electronic spectra of HRgCN and HRgNC (Rg = Xe or Rn)

4.1 Introduction

In this chapter, the focus will be on the rare gas compounds of the form HRgY where Rg = Xe or Rn, and Y = CN or NC (instead of Rg = Ar, Kr, Xe, Rn and Y = F as in the previous chapter). Petterson *et al.* were the first to synthesize HXeCN and HXeNC (as well as HKrCN) [5]. The synthesis was achieved via the photolysis of HCN within a Xe matrix (Kr for HKrCN) at 7.5 K with a 193 nm laser. The subsequent production of hydrogen atoms and CN radicals was then activated by annealing the Xe matrix at 50 K (30 K for Kr). The activated H atoms and CN radicals reacted with the Xe atoms to produce HXeCN and HXeNC. When irradiated with IR radiation, HXeNC converted to HXeCN, with the barrier to isomerization calculated using the MP2 method to be only 0.2 eV [5]. The energy difference (dissociation energy) between HXeCN and HCN+Xe was 4.24 eV [5]. HXeNC photodissociates into HCN + Xe at 350 nm as determined by studying the change in intensity of the peaks in the IR spectrum [5]. Unlike HXeNC, HXeCN is stable and does not photodissociate.

Juarez *et al.* analyzed the energy barrier for two decomposition pathways: HRnY $\rightarrow$ Rn + HY (two body channel) and HRnY $\rightarrow$ H + Rn + Y (three body channel),

where Y = F, Cl, Br, I, CCH, CN, and NC [89]. The systems HRnCN and HRnNC had the two body dissociation barrier of 31.7 kcal/mol and 27.8 kcal/mol, respectively. The three body dissociation barriers for HRnCN and HRnNC were 35.2 kcal/mol and 31.3 kcal/mol, respectively. Khriachtchev *et al.* studied the H/D kinetic isotope effects (KIE) on the formation and dissociation of HKrCl and found that the reaction rates were slower after deuteration [90].

Berski *et al.* used the electron localization function and found that bonding in HRgCN (Rg = Kr, Xe) exhibits charge-transfer character [91]. They found that the isomerization of HRgCN to HRgNC increased the charge separation. The larger stability of HXeCN, as compared to HXeNC, was attributed to the interaction between the lone pair on the C atom and the nonbonding electron density on Xe.

Zhang *et al.* employed natural bond orbital and natural resonance theory and found that the HRgY systems (with Rg = He, Ne, Kr, Xe, Rn and Y = CN, NC) contain ω-bonding and long-bonding resonance [92]. Zhang *et al.* also studied geometry, dissociation energies, and donor-acceptor interactions (stabilization energies) of many HRgY compounds including HXeCN, HXeNC, HRnCN, and HRnNC [93]. The dissociation reactions investigated were HRgAB $\rightarrow$ $HRg^+ + AB^-$ and HRgAB $\rightarrow$ Rg + HAB. The three main donor-acceptor interactions were the lone pair on A to the anti-bonding orbital on H-Rg ($n_A \rightarrow \sigma^*_{H-Rg}$), the lone pair on H to the anti-bonding orbital on Rg-A ($n_H \rightarrow \sigma^*_{Rg-A}$), and the lone pair on Rg to the anti-bonding orbital on H-A ($n_{Rg} \rightarrow \sigma^*_{H-Rg}$).

Experimental VUV spectra were obtained for HXeY (Y= Cl, Br, I, CN) by Ahokas *et al.*, who also studied excited states with multireference configuration interaction [2]. They assigned the broad peak at 250-300 nm to HXeY (Y= Cl, Br, I, CN) because during the synthesis of HXeY this peak increases in intensity as the H/Xe peak at 200 nm decreases in intensity. Because HXeY photodissociates, one can expect HXeY to have strong electronic transitions and therefore a pronounced electronic spectrum. There was a very good correlation between the broad band UV and IR peaks during

the photolysis and annealing cycles, suggesting that the two peaks belong to the same molecule.

In the previous chapter, the electronic spectra of HRgF (Rg = Ar, Kr, Xe, Rn) using the TDDFT(CAMB3LYP) approach were presented [6, 33]. In this present chapter, a comprehensive study of HRgCN and HRgNC (Rg = Xe, Rn) where the structure, VUV, reaction energetics, and KIE are presented. The geometry was optimized for HRgCN and HRgNC (Rg = Xe, Rn) to locate the minima of the potential energy surface as well as at the first-order saddle points corresponding to transition state structures. The kinetic isotope effects were also investigated for the two-body dissociation and isomerization reactions. As was done for HRgF (Rg = Ar, Kr, Xe, Rn) in Chapter 3, the VUV spectra for HRgY (Rg = Xe, Rn and Y = CN, NC) were computed, and the nature of the electronic transitions was analyzed in terms of the molecular orbitals involved in the transitions belonging to the first three excited states with nonzero oscillator strengths. The effect of relativistic effects (spin-orbit coupling) on the VUV spectra are also included.

4.2 Methods and procedure

The geometry optimizations were carried out at the MP2 and DFT(PBE0) levels of theory using four model core potential [67] basis sets: IMCP-SR2 (ims2) [37], IMCP-SR3 (ims3), ZFK3-DK3 (zfk3) [39], and ZFK4-DK3 (zfk4) [39] (the strings in parentheses are abbreviations). The new basis set ims3 was created in this work by adding polarization functions to the basis set ims2 to improve accuracy of the results while saving on CPU time when compared with the zfk3 and zfk4 basis sets. The zfk4 results were used as reference to calculate the errors in the bond lengths and angles for the other basis sets. The systems for which the geometry was optimized were HCN, HNC, HRgY, HRgY-d (the two-channel dissociation transition state, yielding Rg + HY as products), and HRgY-i (the HRgCN to HRgNC isomerization transition state) where Rg = Xe, Rn and Y = CN, NC. The ΔG values were evaluated for the

isomerization and dissociation reactions. The KIEs were computed at the MP2 level of theory with basis sets ims3, zfk3, and zfk4. Both the dissociation reaction and isomerization reactions were investigated at 50 K.

Only the first four non-zero intensity transitions in HRgY were investigated with the TDDFT method [69, 70]: two Σ states and two degenerate components of a Π state. The origins of the peaks were investigated by studying the molecular orbitals involved and the atomic orbital contributions that make up those molecular orbitals. Compatibility of TDDFT implementations as well as basis sets was investigated using three program packages and four all-electron basis sets. With the program package ORCA [53, 54], the functionals used were B2PLYP [29] and B3LYP [31, 94–97] with the basis sets ANO-RCC [98] (only with B2PLYP), Sapporo-QZP-DKH3-2012 (SPKQ) [40], and Sapporo-TZP-DKH3-2012 (SPKT) [41] (abbreviations for basis set names are shown in parentheses). With the program package GAMESS-US [52], the functional B3LYP was used with basis sets SPKT and SPKQ. With the program package ADF [55], the combination of B3LYP functional and QZ4P basis set [47] was used mainly to study the effect of spin-orbit coupling on the spectrum. Table 4.1 shows the combination of functionals and basis sets used as well as the programs that were used. The spectra were simulated with Cauchy-Lorentz functions with a full width at half maximum at 0.3 eV.

Table 4.1: Functionals, basis sets, and programs used in this study (o = ORCA, g = GAMESS-US, a = ADF).

functional (program)	ANO-RCC	SPKQ	SPKT	QZ4P
B2PLYP (o)	✓	✓	✓	-
B3LYP (o)	-	✓	✓	-
B3LYP (g)	-	✓	✓	-
B3LYP (a)	-	-	-	✓

4.3 Results and discussion

4.3.1 Electronic spectra of HRgCN and HRgNC

The order of excited states in HRgCN is $1^1\Pi$, $1\,^1\Sigma^+$, and $2\,^1\Sigma^+$ while for HRgNC it is $1\,^1\Sigma^+$, $1^1\Pi$ (which has a negligible oscillator strength), and $2\,^1\Sigma^+$. Figure 4.1 shows electronic transitions and the five molecular orbitals involved in the transitions: the highest occupied molecular orbital (HOMO, or H), the two degenerate molecular orbitals with orbital energies slightly lower than that of HOMO (HOMO-1 or H-1, and HOMO-2 or H-2), the lowest unoccupied molecular orbital (LUMO, or L), and the next unoccupied molecular orbital (LUMO+1 or L+1). For HRgCN, the first excitation (denoted 1 in figure 4.1) with the lowest energy, is the transition $X^1\Sigma^+ \rightarrow 1^1\Pi$ that involves one-electron excitations from HOMO-1 or HOMO-2 (H-1, H-2) to LUMO. The next is the transition (2) to the $1\,^1\Sigma^+$ state, involves the HOMO-LUMO (H-L) excitation. For HRgCN, this transition corresponds to the most prominent peak. The last, highest energy, transition (3) is the HOMO (H) to LUMO+1 (L+1) excitation leading to the $2\,^1\Sigma^+$ state. For HRgNC, the lowest energy transition (1) is the H-L transition, which leads to the most prominent peak and it occurs at a much lower energy in the spectrum than that for HRgCN. The next transition (2) is the H-1 (or H-2) with a very low intensity, leading to the $1^1\Pi$ state. The last transition (3) for HRgNC is also the H to L+1 transition, same as for HRgCN, and involving the $2\,^1\Sigma^+$ state.

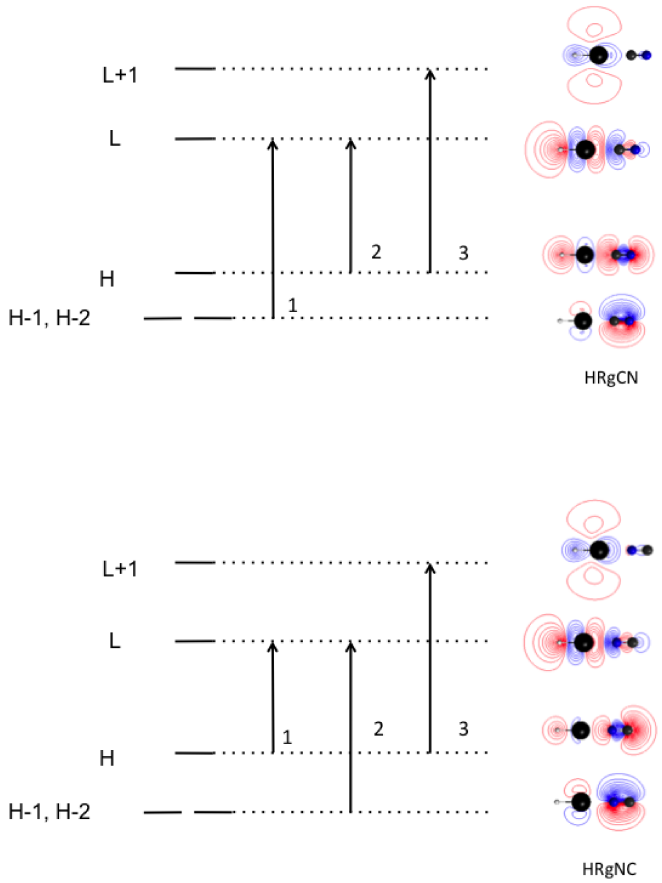

Figure 4.1: Frontier molecular orbitals of HRgCN and HRgNC: HOMO-2 (H-2), HOMO-1 (H-1), HOMO (H), LUMO (L), and LUMO+1 (L+1) as well as the main transitions (1, 2, 3).

The composition of the orbitals involved in the electronic excitations is very similar for all the HRgY compounds (figure 4.1). The HOMO-1 and HOMO-2 orbitals are degenerate and composed mostly of either a p_y or p_x atomic orbitals (AO) positioned on the C and N atoms. The HOMO and LUMO orbitals consist of s and p_z AO contributed by all atoms. The HOMO has more of its electron density located near the C end for HRgNC and the N end for HRgCN as when compared to the LUMO. The LUMO has most of its electron density at the H end and much less electron density at the other end of the molecule. The LUMO+1 is composed of s, p_z and d_{z^2} AO, the most diffuse of which are centred on the Rg atom.

Figure 4.2 shows the computed spectra for HRgCN (in red) and the HRgNC (in blue) using the SPKQ basis set. The top panels show the spectra for HXeY and the bottom panels show the spectra for HRnY. The first column shows the spectra computed with B2PLYP in ORCA (B2PLYP(o)), the middle column with B3LYP in ORCA (B3LYP(o)), and the third column with B3LYP in GAMESS-US (B3LYP(g)). The spectrum of HRgNC starts at lower energies, and with a smaller oscillator strength than in the HRgCN case. The most prominent peak for HRgCN is blue-shifted ($\sim$6 eV) compared to the most prominent peak of HRgNC ($\sim$4.5 eV). The prominent peaks in the spectra of both HRgCN and HRgNC are due to the HOMO-LUMO transitions. When using the B2PLYP functional in ORCA, the excitation to the $2\,^1\Sigma^+$ state of HRgCN has a large oscillator strength, creating a second peak near the $1\,^1\Sigma^+$ peak instead of creating a slight shoulder like it does when using B3LYP in ORCA or GAMESS-US. The excitation to the $1^1\Pi$ state has such low oscillator strength that it is not noticeable in the spectra. The positions of the peaks are very similar whether using B2PLYP(o) or B3LYP(o). The B3LYP(g) spectrum is red-shifted relative to B2PLYP(o) and B3LYP(o) by about 0.2 eV. The excitation energies and intensities decrease upon substitution of CN by NC, but the energies do not change much when Xe is replaced by Rn. The spectra of HXeY are very similar of those of HRnY provided that only scalar relativistic effects are included.

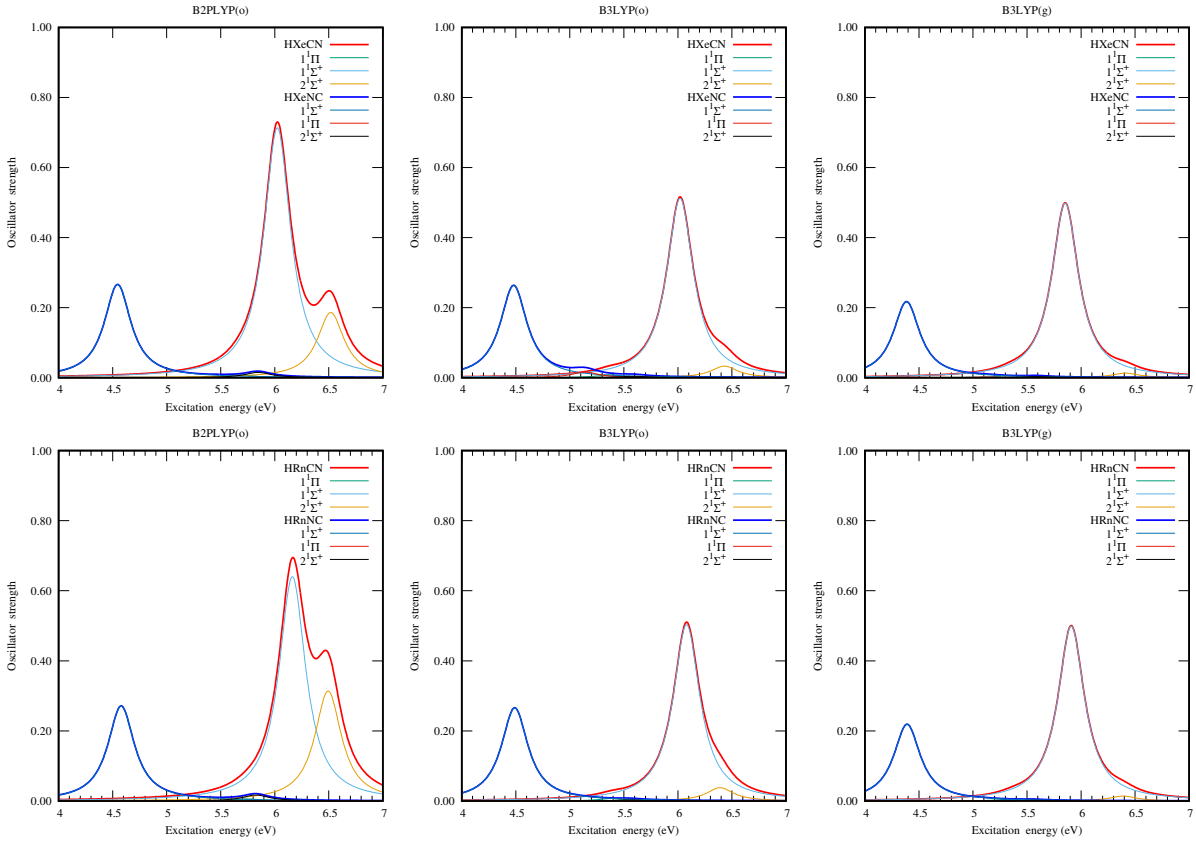

Figure 4.2: TDDFT spectra of the HRgCN and HRgNC using either B2PLYP or B3LYP in ORCA(o) or GAMESS-US(g).

Comparison of results obtained with B2PLYP(o) using the ANO-RCC, SPKQ, and SPKT basis sets for each HRgY molecule shows (table 4.2) that the results for HXeCN are very similar (0.01 - 0.10 eV difference) regardless of basis set. The larger difference (0.10 eV) occurred in all HRgY systems for the $2\,^1\Sigma^+$ state (with the SPKQ basis set).

Table 4.2: Excitation state data for HRgY (Rg = Xe, Rn and Y = CN, NC) at the B2PLYP level of theory using ORCA with three different basis sets. Energies (ΔE) are in eV and wavelengths (λ) are in nm.

				HXeCN					
	ANO-RCC			SPKQ			SPKT		
State	ΔE	λ	f	ΔE	λ	f	ΔE	λ	f
$1\,^1\Pi$	5.69	218	0.008	5.69	218	0.008	5.66	219	0.008
$1\,^1\Sigma^+$	6.03	206	0.745	6.02	206	0.713	6.00	207	0.752
$2\,^1\Sigma^+$	6.63	187	0.168	6.52	190	0.186	6.56	189	0.145
				HXeNC					
$1\,^1\Sigma^+$	4.55	272	0.268	4.55	273	0.266	4.54	273	0.267
$1\,^1\Pi$	5.51	225	0.001	5.51	225	0.001	5.49	226	0.001
$2\,^1\Sigma^+$	5.96	208	0.016	5.85	212	0.015	5.92	209	0.016
				HRnCN					
$1\,^1\Pi$	5.74	216	0.006	5.74	216	0.006	5.71	217	0.006
$1\,^1\Sigma^+$	6.15	202	0.700	6.16	201	0.640	6.15	202	0.656
$2\,^1\Sigma^+$	6.59	188	0.264	6.49	191	0.314	6.50	191	0.300
				HRnNC					
$1\,^1\Sigma^+$	4.59	270	0.272	4.58	271	0.271	4.57	271	0.271
$1\,^1\Pi$	5.51	225	0.001	5.51	225	0.001	5.51	225	0.001
$2\,^1\Sigma^+$	5.93	209	0.015	5.83	213	0.017	5.87	211	0.018

Table 4.3 compares the B3LYP results obtained with two basis sets and two programs: SPKX(o) and SPKX(g), where X= T or Q. Comparisons between SPKX(o) and SPKX(g) show that for all four HRgY systems, the largest difference of 0.17 eV is found for the excitation to the $1\,^1\Sigma^+$ state (the other states have much smaller differences, close to 0.01 eV). Compared with results at the B2PLYP level of theory (table 4.2), the B3LYP excitation energies tend to be larger. In the experimental VUV spectrum of HCN/Xe, Ahokas *et al.* assigned the broad band at 5.30 eV to HXeCN [2]. Our reported $1\,^1\Sigma^+$ excitation energy of $\sim$6 eV is too high and our reported $1\,^1\Sigma^+$ excitation energy of $\sim$4.5 eV for HXeNC is too low when compared to the experimental peak at 5.30 eV.

Table 4.3: Excitation state data for HRgY (Rg = Xe, Rn and Y = CN, NC) at the B3LYP level of theory using either ORCA or GAMESS-US and SPKQ or SPKT. Energies (ΔE) are in eV and wavelengths (λ) are in nm.

	HXeCN											
	SPKQ(o)			SPKQ(g)			SPKT(o)			SPKT(g)		
State	ΔE	λ	f	ΔE	λ	f	ΔE	λ	f	ΔE	λ	f
$1\,^1\Pi$	5.37	231	0.008	5.36	231	0.007	5.39	230	0.008	5.36	231	0.007
$1\,^1\Sigma^+$	6.02	206	0.512	5.85	212	0.498	6.02	206	0.523	5.86	212	0.503
$2\,^1\Sigma^+$	6.43	193	0.033	6.41	193	0.013	6.48	191	0.024	6.47	192	0.010
	HXeNC											
$1\,^1\Sigma^+$	4.48	277	0.263	4.39	282	0.217	4.48	277	0.264	4.39	282	0.217
$1\,^1\Pi$	5.15	241	0.002	5.13	242	0.001	5.15	241	0.002	5.13	242	0.001
$2\,^1\Sigma^+$	5.58	222	0.004	5.58	222	0.003	5.69	218	0.004	5.69	218	0.003
	HRnCN											
$1\,^1\Pi$	5.39	230	0.007	5.37	231	0.006	5.39	230	0.007	5.37	231	0.005
$1\,^1\Sigma^+$	6.08	204	0.503	5.91	210	0.499	6.08	204	0.507	5.91	210	0.501
$2\,^1\Sigma^+$	6.39	194	0.038	6.39	194	0.014	6.42	193	0.036	6.41	193	0.014
	HRnNC											
$1\,^1\Sigma^+$	4.49	276	0.266	4.39	282	0.219	4.49	276	0.267	4.39	282	0.220
$1\,^1\Pi$	5.12	242	0.001	5.11	243	0.001	5.12	242	0.001	5.11	243	0.001
$2\,^1\Sigma^+$	5.56	223	0.003	5.55	223	0.002	5.61	221	0.003	5.60	221	0.002

Figure 4.3 shows the spectra of HRgY obtained at the B3LYP/QZ4P level of theory using the program package ADF. The excitation data is shown in table 4.4. Including SOC had little impact on the spectra of HXeY. However, for HRnCN, the spin-orbit

coupling red-shifted the most prominent peak while for HRnNC spin-orbit coupling blue-shifted the most prominent peak, and created a few smaller peaks.

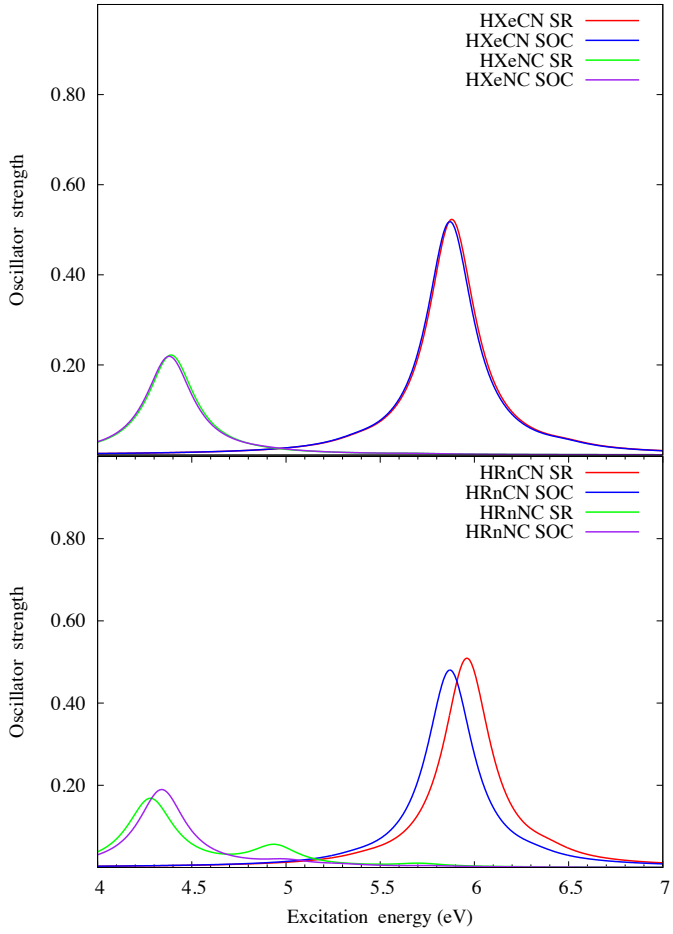

Figure 4.3: Electronic spectra of HRgY at the B3LYP/QZ4P level of theory using ADF (SR = scalar relativistic and SOC = spin-orbit coupling).

Table 4.4: Excitation state data for HRgY (Rg = Xe, Rn and Y = CN, NC) at the TDDFT/B3LYP/QZ4P level of theory using ADF. Energies (ΔE) are in eV and wavelengths (λ) are in nm. SR = scalar relativistic, SOC = spin-orbit coupling.

HXeCN							
SR				SOC			
State	ΔE	λ	f	State	ΔE	λ	f
$1\,^1\Pi$	5.38	231	0.007	$1\,\Pi$	5.37	231	0.007
$1\,^1\Sigma^+$	5.88	211	0.522	$1\,\Sigma^+$	5.87	211	0.517
$2\,^1\Sigma^+$	6.49	191	0.007	$2\,\Sigma^+$	6.48	191	0.006
HXeNC							
$1\,^1\Sigma^+$	4.39	283	0.222	$1\,\Sigma^+$	4.38	283	0.219
-	-	-	-	$2\,\Sigma^+$	4.90	253	0.002
$2\,^1\Sigma^+$	5.68	218	0.001	$3\,\Sigma^+$	5.68	218	0.001
$1\,^1\Pi$	6.92	179	0.022	$1\,\Pi$	6.88	180	0.004
HRnCN							
$1\,^1\Pi$	5.42	229	0.005	$1\,\Pi$	5.36	231	0.005
$1\,^1\Sigma^+$	5.96	208	0.507	$1\,\Sigma^+$	5.87	211	0.479
$2\,^1\Sigma^+$	6.39	194	0.016	$2\,\Sigma^+$	6.32	196	0.009
HRnNC							
$1\,^1\Sigma^+$	4.28	290	0.166	$1\,\Sigma^+$	4.34	286	0.189
$2\,^1\Sigma^+$	4.94	251	0.048	$2\,\Sigma^+$	5.00	248	0.011
$3\,^1\Sigma^+$	5.71	217	0.007	$3\,\Sigma^+$	5.30	234	0.003
-	-	-	-	$4\,\Sigma^+$	5.77	215	0.001
$1\,^1\Pi$	6.99	178	0.072	$1\,\Pi$	5.14	241	0.001

4.3.2 Geometry optimization: average absolute errors for each type of bond angle due to basis set effects

The results of the assessment of the efficacy of the new basis set (table 4.5) show that the overall accuracy increases in the order ims2, ims3, and zfk3. The ims3 basis set is significantly better than ims2 in predicting geometrical structure of the molecules studied here, being almost as good as zfk3 at both the MP2 and PBE0 levels of theory. The errors in the bond lengths found with the ims2 basis set are 3-4 times larger than the ones found using the ims3 basis set (the only exceptions are H-Rn, C-N, and N-C bond). The errors in the ims3 bond lengths are 2-4 times larger than the ones found for the zfk3 basis set, while the bond angles errors are an order of magnitude larger than the zfk3 values. The raw data that were used in computing the average absolute errors (AAE) in table 4.5 are collected in tables 4.6- 4.9 for the MP2 results and tables 4.10- 4.13 for the DFT(PBE0) results. Tables 4.14 and 4.15 collect the AAE values for individual bonds and angles.

Table 4.5: Average absolute errors (AAE) for structural parameters relative to zfk4 values.

	method	ims2	ims3	zfk3
bonds	MP2	0.0204	0.0054	0.0028
	PBE0	0.0167	0.0056	0.0013
angles	MP2	2.57	0.78	0.07
	PBE0	2.14	0.48	0.05

$^{(a)}$ bond lengths in Å, bond angles in degrees

Table 4.6: MP2 values of structural parameters of HY systems.[a,b]

	HCN	
basis	H-C	C-N
ims2	1.0513 (-.0124)	1.1638 (.0019)
ims3	1.0643 (.0006)	1.1650 (.0031)
zfk3	1.0652 (.0015)	1.1646 (.0027)
zfk4	1.0637	1.1619
	HNC	
basis	H-N	N-C
ims2	0.9864 (-.0096)	1.1722 (.0006)
ims3	0.9974 (.0014)	1.1729 (.0013)
zfk3	0.9973 (.0013)	1.1743 (.0027)
zfk4	0.9960	1.1716

[a] bond lengths in Å; [b] The values in parentheses are differences with respect to the MP2/zfk4 values: $\mathcal{P}$(MP2/basis) - $\mathcal{P}$(MP2/zfk4)

Table 4.7: MP2 values of structural parameters of HRgY systems.[a,b]

	HXeCN		
basis	H-Xe	Xe-C	C-N
ims2	1.7032 (-.0046)	2.3857 (-.0122)	1.1781 (.0026)
ims3	1.7111 (.0033)	2.4113 (.0134)	1.1795 (.0040)
zfk3	1.7087 (.0009)	2.4010 (.0031)	1.1782 (.0027)
zfk4	1.7078	2.3979	1.1755
	HXeNC		
basis	H-Xe	Xe-N	N-C
ims2	1.6503 (-.0106)	2.3463 (.0128)	1.1865 (.0017)
ims3	1.6634 (.0025)	2.3449 (.0114)	1.1869 (.0021)
zfk3	1.6612 (.0003)	2.3363 (.0028)	1.1873 (.0025)
zfk4	1.6609	2.3335	1.1848
	HRnCN		
basis	H-Rn	Rn-C	C-N
ims2	1.8215 (.0137)	2.4714 (.0100)	1.1782 (.0030)
ims3	1.8231 (.0153)	2.4702 (.0088)	1.1792 (.0040)
zfk3	1.8093 (.0015)	2.4631 (.0017)	1.1778 (.0026)
zfk4	1.8078	2.4614	1.1752
	HRnNC		
basis	H-Rn	Rn-N	N-C
ims2	1.7688 (.0073)	2.4238 (.0283)	1.1854 (.0012)
ims3	1.7730 (.0115)	2.4024 (.0069)	1.1866 (.0024)
zfk3	1.7624 (.0009)	2.3973 (.0018)	1.1867 (.0025)
zfk4	1.7615	2.3955	1.1842

[a] bond lengths in Å; [b] The values in parentheses are differences with respect to the MP2/zfk4 values: $\mathcal{P}$(MP2/basis) - $\mathcal{P}$(MP2/zfk4)

Table 4.8: MP2 values of structural parameters at the transition states for two-channel dissociation in HRgY systems.[a,b,c]

	HXeCN-*d*				
basis	H-Xe	Xe-C	C-N	H-Xe-C	Xe-C-N
ims2	1.5783 (-.0141)	3.0647 (.1074)	1.1865 (.0020)	112.14 (1.89)	77.32 (-1.29)
ims3	1.5892 (-.0032)	2.9500 (-.0073)	1.1867 (.0022)	110.38 (.13)	78.90 (.29)
zfk3	1.5925 (.0001)	2.9646 (.0073)	1.1872 (.0027)	110.14 (-.11)	78.63 (.02)
zfk4	1.5924	2.9573	1.1845	110.25	78.61
	HXeNC-*d*				
basis	H-Xe	Xe-N	N-C	H-Xe-N	Xe-N-C
ims2	1.5779 (-.0138)	2.9212 (.0652)	1.1874 (.0020)	111.27 (.63)	92.13 (3.41)
ims3	1.5884 (-.0033)	2.8600 (.0040)	1.1875 (.0021)	111.25 (.61)	87.76 (-.96)
zfk3	1.5918 (.0001)	2.8651 (.0091)	1.1880 (.0026)	110.64 (.00)	88.56 (-.16)
zfk4	1.5917	2.8560	1.1854	110.64	88.72
	HRnCN-*d*				
basis	H-Rn	Rn-C	C-N	H-Rn-C	Rn-C-N
ims2	1.6806 (-.0006)	3.1382 (.1249)	1.1866 (.0019)	107.25 (2.82)	77.59 (-1.07)
ims3	1.6839 (.0027)	3.0179 (.0046)	1.1868 (.0021)	105.72 (1.29)	78.21 (-.45)
zfk3	1.6820 (.0008)	3.0212 (.0079)	1.1874 (.0027)	104.30 (-.13)	78.58 (-.08)
zfk4	1.6812	3.0133	1.1847	104.43	78.66
	HRnNC-*d*				
basis	H-Rn	Rn-N	N-C	H-Rn-N	Rn-N-C
ims2	1.6799 (-.0006)	3.0020 (.0856)	1.1874 (.0019)	106.40 (1.35)	91.76 (3.33)
ims3	1.6834 (.0029)	2.9124 (-.0040)	1.1877 (.0022)	106.04 (.99)	88.86 (.43)
zfk3	1.6813 (.0008)	2.9245 (.0081)	1.1882 (.0027)	104.98 (-.07)	88.33 (-.10)
zfk4	1.6805	2.9164	1.1855	105.05	88.43

[a] bond lengths in Å, bond angles in degrees; [b] The values in parentheses are differences with respect to the MP2/zfk4 values: $\mathcal{P}$(MP2/basis) - $\mathcal{P}$(MP2/zfk4); [c] The dihedral angle H-Rg-A-B=0°

Table 4.9: MP2 values of structural parameters at the transition states for isomerization in HRgY systems.[a,b,c]

	HXeCN-*i*				
basis	H-Xe	Xe-C	C-N	H-Xe-C	Xe-C-N
ims2	1.6386 (-.0157)	2.6819 (.0892)	1.1914 (.0027)	169.96 (-1.27)	78.46 (-3.56)
ims3	1.6548 (.0005)	2.6195 (.0268)	1.1913 (.0026)	170.50 (-.73)	80.63 (-1.39)
zfk3	1.6542 (-.0001)	2.5988 (.0061)	1.1914 (.0027)	171.23 (.00)	82.12 (.10)
zfk4	1.6543	2.5927	1.1887	171.23	82.02
	HXeNC-*i*				
basis	H-Xe	Xe-N	N-C	H-Xe-N	Xe-N-C
ims2	1.6386 (-.0157)	2.7081 (.01)	1.1914 (.0027)	164.50 (1.60)	76.00 (3.89)
ims3	1.6548 (.0005)	2.6954 (-.0027)	1.1913 (.0026)	163.64 (.74)	73.51 (1.40)
zfk3	1.6542 (-.0001)	2.7064 (.0083)	1.1914 (.0027)	162.92 (.02)	72.02 (-.09)
zfk4	1.6543	2.6981	1.1887	162.90	72.11
	HRnCN-*i*				
basis	H-Rn	Rn-C	C-N	H-Rn-C	Rn-C-N
ims2	1.7584 (.0039)	2.7376 (.1080)	1.1914 (.0030)	169.70 (-1.98)	77.74 (-5.24)
ims3	1.7655 (.0110)	2.6447 (.0151)	1.1910 (.0026)	171.06 (-.62)	82.00 (-.98)
zfk3	1.7551 (.0006)	2.6352 (.0056)	1.1911 (.0027)	171.63 (-.05)	82.93 (-.05)
zfk4	1.7545	2.6296	1.1884	171.68	82.98
	HRnNC-*i*				
basis	H-Rn	Rn-N	N-C	H-Rn-N	Rn-N-C
ims2	1.7584 (.0039)	2.7439 (-.0062)	1.1914 (.0030)	165.20 (2.27)	77.15 (5.53)
ims3	1.7655 (.0110)	2.7451 (-.0050)	1.1910 (.0026)	163.50 (.57)	72.56 (.94)
zfk3	1.7551 (.0006)	2.7551 (.0050)	1.1911 (.0027)	162.96 (.03)	71.66 (.04)
zfk4	1.7545	2.7501	1.1884	162.93	71.62

[a] bond lengths in Å, bond angles in degrees; [b] The values in parentheses are differences with respect to the MP2/zfk4 values: $\mathcal{P}$(MP2/basis) - $\mathcal{P}$(MP2/zfk4); [c] The dihedral angle H-Rg-C-N=180°

Table 4.10: PBE0 values of structural parameters of HY systems.[a,b]

	HCN	
basis	H-C	C-N
ims2	1.0655 (.0002)	1.1448 (.0042)
ims3	1.0655 (.0002)	1.1437 (.0031)
zfk3	1.0657 (.0004)	1.1414 (.0008)
zfk4	1.0653	1.1406
	HNC	
basis	H-N	N-C
ims2	0.9926 (-.0016)	1.1620 (.0026)
ims3	0.9934 (-.0008)	1.1603 (.0009)
zfk3	0.9947 (.0005)	1.1603 (.0009)
zfk4	0.9942	1.1594

[a] bond lengths in Å; [b] The values in parentheses are differences with respect to the PBE0/zfk4 values: $\mathcal{P}$(PBE0/basis) - $\mathcal{P}$(PBE0/zfk4)

Table 4.11: PBE0 values of structural parameters of HRgY systems.[a,b]

	HXeCN		
basis	H-Xe	Xe-C	C-N
ims2	1.7178 (-.0012)	2.3747 (-.0293)	1.1577 (.0046)
ims3	1.7183 (-.0007)	2.4190 (.0150)	1.1562 (.0031)
zfk3	1.7206 (.0016)	2.4038 (-.0002)	1.1538 (.0007)
zfk4	1.7190	2.4040	1.1531
	HXeNC		
basis	H-Xe	Xe-N	N-C
ims2	1.6759 (-.0036)	2.3123 (-.0124)	1.1730 (.0048)
ims3	1.6777 (-.0018)	2.3441 (.0194)	1.1706 (.0024)
zfk3	1.6806 (.0011)	2.3251 (.0004)	1.1691 (.0009)
zfk4	1.6795	2.3247	1.1682
	HRnCN		
basis	H-Rn	Rn-C	C-N
ims2	1.8401 (.0237)	2.4527 (-.0116)	1.1576 (.0048)
ims3	1.8284 (.0120)	2.4651 (.0008)	1.1556 (.0028)
zfk3	1.8182 (.0018)	2.4641 (-.0002)	1.1536 (.0008)
zfk4	1.8164	2.4643	1.1528
	HRnNC		
basis	H-Rn	Rn-N	N-C
ims2	1.8001 (.0226)	2.3872 (.0028)	1.1722 (.0044)
ims3	1.7889 (.0114)	2.3863 (.0019)	1.1702 (.0024)
zfk3	1.7792 (.0017)	2.3849 (.0005)	1.1686 (.0008)
zfk4	1.7775	2.3844	1.1678

[a] bond lengths in Å; [b] The values in parentheses are differences with respect to the PBE0/zfk4 values: $\mathcal{P}$(PBE0/basis) - $\mathcal{P}$(PBE0/zfk4)

Table 4.12: PBE0 values of structural parameters at the transition states for two-channel dissociation in HRgY systems.[a,b,c]

	HXeCN-*d*				
basis	H-Xe	Xe-C	C-N	H-Xe-C	Xe-C-N
ims2	1.6150 (.0027)	2.9774 (.0634)	1.1693 (.0043)	105.74 (.36)	83.57 (.64)
ims3	1.6119 (-.0004)	2.9184 (.0044)	1.1678 (.0028)	106.29 (.91)	83.01 (.08)
zfk3	1.6148 (.0025)	2.9156 (.0016)	1.1658 (.0008)	105.33 (-.05)	82.95 (.02)
zfk4	1.6123	2.9140	1.1650	105.38	82.93
	HXeNC-*d*				
basis	H-Xe	Xe-N	N-C	H-Xe-N	Xe-N-C
ims2	1.6109 (.0034)	2.8272 (.0398)	1.1719 (.0046)	105.10 (-1.03)	104.19 (5.39)
ims3	1.6068 (-.0007)	2.7903 (.0029)	1.1700 (.0027)	106.93 (.80)	99.14 (.34)
zfk3	1.6099 (.0024)	2.7886 (.0012)	1.1681 (.0008)	106.09 (-.04)	98.82 (.02)
zfk4	1.6075	2.7874	1.1673	106.13	98.80
	HRnCN-*d*				
basis	H-Rn	Rn-C	C-N	H-Rn-C	Rn-C-N
ims2	1.7346 (.0355)	3.0404 (.0663)	1.1692 (.0041)	100.74 (.40)	83.71 (1.48)
ims3	1.7089 (.0098)	2.9663 (-.0078)	1.1677 (.0026)	101.53 (1.19)	82.58 (.35)
zfk3	1.7022 (.0031)	2.9761 (.0020)	1.1659 (.0008)	100.23 (-.11)	82.29 (.06)
zfk4	1.6991	2.9741	1.1651	100.34	82.23
	HRnNC-*d*				
basis	H-Rn	Rn-N	N-C	H-Rn-N	Rn-N-C
ims2	1.7320 (.0368)	2.8999 (.0490)	1.1715 (.0044)	100.65 (-.81)	102.93 (5.67)
ims3	1.7050 (.0098)	2.8255 (-.0254)	1.1700 (.0029)	101.83 (.37)	100.02 (2.76)
zfk3	1.6984 (.0032)	2.8535 (.0026)	1.1680 (.0009)	101.47 (.01)	97.22 (-.04)
zfk4	1.6952	2.8509	1.1671	101.46	97.26

[a] bond lengths in Å, bond angles in degrees; [b] The values in parentheses are differences with respect to the PBE0/zfk4 values: $\mathcal{P}$(PBE0/basis) - $\mathcal{P}$(PBE0/zfk4); [c] The dihedral angle H-Rg-A-B=0°

Table 4.13: PBE0 values of structural parameters at the transition states for isomerization in HRgY systems.[a,b,c]

	HXeCN-*i*				
basis	H-Xe	Xe-C	C-N	H-Xe-C	Xe-C-N
ims2	1.6730 (-.0050)	2.6140 (.0458)	1.1748 (.0056)	170.25 (-1.17)	80.71 (-2.88)
ims3	1.6777 (-.0003)	2.5790 (.0108)	1.1719 (.0027)	171.57 (.15)	83.83 (.24)
zfk3	1.6799 (.0019)	2.5701 (.0019)	1.1701 (.0009)	171.38 (-.04)	83.53 (-.06)
zfk4	1.6780	2.5682	1.1692	171.42	83.59
	HXeNC-*i*				
basis	H-Xe	Xe-N	N-C	H-Xe-N	Xe-N-C
ims2	1.6730 (-.0049)	2.6876 (-.0124)	1.1748 (.0055)	164.16 (1.05)	73.71 (2.75)
ims3	1.6778 (-.0001)	2.7160 (.0160)	1.1719 (.0026)	163.00 (-.11)	70.75 (-.21)
zfk3	1.6799 (.0020)	2.7009 (.0009)	1.1701 (.0008)	163.14 (.03)	71.01 (.05)
zfk4	1.6779	2.7000	1.1693	163.11	70.96
	HRnCN-*i*				
basis	H-Rn	Rn-C	C-N	H-Rn-C	Rn-C-N
ims2	1.8000 (.0247)	2.6527 (.0514)	1.1747 (.0062)	170.56 (-1.54)	81.38 (-3.93)
ims3	1.7895 (.0142)	2.5967 (-.0046)	1.1714 (.0029)	172.01 (-.09)	85.33 (.02)
zfk3	1.7774 (.0021)	2.6035 (.0022)	1.1694 (.0009)	172.05 (-.05)	85.22 (-.09)
zfk4	1.7753	2.6013	1.1685	172.10	85.31
	HRnNC-*i*				
basis	H-Rn	Rn-N	N-C	H-Rn-N	Rn-N-C
ims2	1.8000 (.0247)	2.7354 (-.0277)	1.1747 (.0062)	164.32 (1.35)	73.50 (3.73)
ims3	1.7895 (.0142)	2.7602 (-.0029)	1.1714 (.0029)	162.97 (.00)	69.66 (-.11)
zfk3	1.7774 (.0021)	2.7636 (.0005)	1.1694 (.0009)	163.01 (.04)	69.85 (.08)
zfk4	1.7753	2.7631	1.1685	162.97	69.77

[a] bond lengths in Å, bond angles in degrees; [b] The values in parentheses are differences with respect to the PBE0/zfk4 values: $\mathcal{P}$(PBE0/basis) - $\mathcal{P}$(PBE0/zfk4); [c] The dihedral angle H-Rg-C-N=180°

Table 4.14: MP2 average absolute errors in bond lengths (in Å) and angles (in degrees).

bonds	ims2	ims3	zfk3
H-C	0.0124	0.0006	0.0015
H-N	0.0096	0.0014	0.0013
C-N	0.0024	0.0029	0.0027
N-C	0.0019	0.0022	0.0026
H-Xe	0.0124	0.0022	0.0003
Xe-C	0.0696	0.0158	0.0055
Xe-N	0.0293	0.0060	0.0067
H-Rn	0.0050	0.0091	0.0009
Rn-C	0.0810	0.0095	0.0051
Rn-N	0.0400	0.0053	0.0050
angles	ims2	ims3	zfk3
H-Xe-C	1.58	0.43	0.05
H-Xe-N	1.11	0.67	0.01
Xe-C-N	2.42	0.84	0.06
Xe-N-C	3.65	1.18	0.12
H-Rn-C	2.40	0.95	0.09
H-Rn-N	1.81	0.78	0.05
Rn-C-N	3.15	0.71	0.06
Rn-N-C	4.43	0.68	0.07

Table 4.15: PBE0 average absolute errors in bond lengths (in Å) and angles (in degrees).

bonds	ims2	ims3	zfk3
H-C	0.0002	0.0002	0.0004
H-N	0.0016	0.0008	0.0005
C-N	0.0048	0.0029	0.0008
N-C	0.0046	0.0024	0.0009
H-Xe	0.0035	0.0007	0.0019
Xe-C	0.0462	0.0101	0.0012
Xe-N	0.0215	0.0128	0.0008
H-Rn	0.0280	0.0119	0.0023
Rn-C	0.0431	0.0044	0.0015
Rn-N	0.0265	0.0101	0.0012
angles	ims2	ims3	zfk3
H-Xe-C	0.76	0.53	0.04
H-Xe-N	1.04	0.45	0.03
Xe-C-N	1.76	0.16	0.04
Xe-N-C	4.07	0.27	0.03
H-Rn-C	0.97	0.64	0.08
H-Rn-N	1.08	0.18	0.02
Rn-C-N	2.70	0.18	0.07
Rn-N-C	4.70	1.43	0.06

The CPU timing comparisons (for direct SCF and MP2 on a single core) were done for the HRgCN systems and are shown in table 4.16. For these systems the zfk3 basis set gives the closest results to the zfk4 basis set. The SCF, MP2 energy, and MP2 gradient calculations for the zfk3 basis are 3-4 times faster than those using the zfk4 basis set while giving results of satisfactory qualities (table 4.5): the ims3 basis set is still sufficiently for this work while offering significant savings in CPU time.

Table 4.16: CPU time (in seconds) for HXeCN and HRnCN at the MP2 level of theory. K is the number of contracted basis functions, SCF is the time per one SCF iteration, Energy is the time needed to compute the MP2 correction to the total energy, and Gradient is the time needed to calculate the MP2 gradient. The values in parentheses show how many times faster is a given computational step compared to the same step in the zfk4 basis set.

basis set	K	SCF	Energy	Gradient
		HXeCN		
ims2	91	0.9 (202)	4.1 (196)	14.5 (172)
ims3	145	3.2 (56.9)	14.8 (54.4)	61.1 (40.8)
zfk3	239	57.4 (3.17)	236.3 (3.40)	678.6 (3.67)
zfk4	347	182.2 (1.00)	804.8 (1.00)	2494.3 (1.00)
		HRnCN		
ims2	91	0.5 (203)	4.2 (197)	15.4 (166)
ims3	145	1.8 (56.4)	15.3 (54.0)	62.3 (41.1)
zfk3	234	32.8 (3.10)	249.7 (3.31)	728.9 (3.51)
zfk4	342	101.6 (1.00)	826.3 (1.00)	2559.8 (1.00)

4.3.3 Reaction energetics: stability and kinetic isotope effects

In the isomerization reaction both the product and reactant are linear while the transition state structure is T-shaped, with almost a 90 degrees angle between the HRn and CN fragments (figure 4.4 (b)). In the transition state, a new bond is formed between Rg (black) and C (grey) while the Rg and N (blue) bond is being broken to form the HRgCN product (figure 4.4 (c)). For the HRgCN dissociation transition state (figure 4.5), the Rg-H bond (black and white atoms) is being broken while the H is attaching to the N (blue) atom to form the dissociation products Rg + HNC.

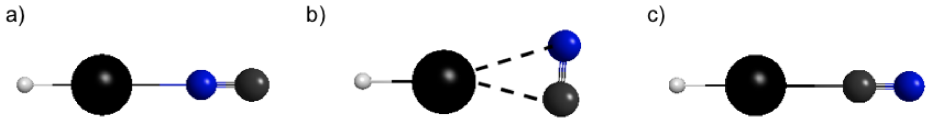

Figure 4.4: Molecular geometry at stationary points for isomerization reaction: (a) HRnNC, (b) transition state, (c) HRnCN.

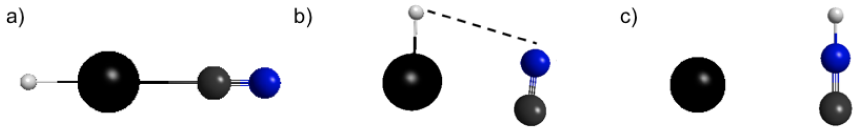

Figure 4.5: Molecular geometry at stationary points in dissociation reaction: (a) HRnCN, (b) transition state, (c) Rn + HNC.

It was confirmed by following the intrinsic reaction coordinate trajectory that the dissociation of HRgCN leads to the products Rg and HNC (and not HCN although further isomerization may lead to this product) (equation 4.1). Similarly, HRgNC dissociates to HCN (equation 4.2).

$$\mathrm{HRgCN} \rightarrow [\mathrm{HRgCN}]^{\ddagger} \rightarrow \mathrm{HNC} + \mathrm{Rg} \tag{4.1}$$

$$\mathrm{HRgNC} \rightarrow [\mathrm{HRgNC}]^{\ddagger} \rightarrow \mathrm{HCN} + \mathrm{Rg} \tag{4.2}$$

The values of the free energy change ΔG for the reactions studied at the MP2 and DFT/PBE0 level of theory are shown tables 4.17 and 4.18, respectively. These results allow for comparison of the ΔG values computed using the ims3 basis with those obtained using the zfk3 and zfk4 basis sets. The average absolute errors in ΔG, shown in table 4.19 illustrate that ims3 is significantly better than ims2 by a factor of five (for MP2) and three (for PBE0). The ims3 ΔG results are still not as accurate as the zfk3 results, in particular at the PBE0 level of theory. Some exceptions exist at the MP2 level of theory where the ims3 basis occasionally leads to a larger AAE than that found for ims2 (table 4.17). These exception occur for reactions of HCN $\rightarrow$ HNC, HXeNC $\rightarrow$ HXeNC-*d*, HRnCN $\rightarrow$ HRnNC, and HRnCN $\rightarrow$ HRnCN-*d* (where *d* stands for the dissociation transition state). At the PBE0 level of theory (table 4.18) the ims3 error is greater than the ims2 one only in two reactions: HXeNC $\rightarrow$ HXeNC-*d* and HRnCN $\rightarrow$ HRnCN-*d*.

Table 4.17: Gibbs free energy change (ΔG) and errors in ΔG ($\Delta\Delta G$) with respect to zfk4 values at the MP2 level of theory.[a] All values are in kJ/mol.

reaction			ims2		ims3		zfk3		zfk4
			ΔG	$\Delta\Delta G$	ΔG	$\Delta\Delta G$	ΔG	$\Delta\Delta G$	ΔG
HCN	→	HNC	73.58	(-.21)	67.84	(-5.95)	73.88	(0.09)	73.79
HXeCN	→	HXeNC	26.66	(4.64)	25.11	(3.09)	22.98	(0.96)	22.02
HXeNC	→	HXeCN-*i*	20.82	(9.90)	11.27	(0.35)	10.68	(-0.24)	10.92
HXeCN	→	HXeCN-*i*	47.48	(14.54)	36.38	(3.44)	33.66	(0.72)	32.94
HXeCN	→	HXeCN-*d*	126.00	(3.42)	123.75	(1.17)	122.59	(0.01)	122.58
HXeNC	→	HXeNC-*d*	98.12	(-1.65)	97.94	(-1.83)	98.80	(-0.97)	99.77
HRnCN	→	HRnNC	26.85	(3.07)	27.67	(3.89)	24.81	(1.03)	23.78
HRnNC	→	HRnCN-*i*	19.88	(12.40)	10.16	(2.68)	7.57	(0.09)	7.48
HRnCN	→	HRnCN-*i*	46.73	(15.47)	37.83	(6.57)	32.38	(1.12)	31.26
HRnCN	→	HRnCN-*d*	137.16	(1.58)	140.91	(5.33)	136.41	(0.83)	135.58
HRnNC	→	HRnNC-*d*	109.29	(-2.07)	112.71	(1.35)	133.94	(22.58)	111.36
HXeCN	→	Xe + HNC	-404.28	(-29.13)	-379.36	(-4.21)	-371.25	(3.90)	-375.15
HXeNC	→	Xe + HCN	-504.52	(-33.56)	-472.31	(-1.35)	-468.11	(2.85)	-470.96
HXeCN-*d*	→	Xe + HNC	-530.28	(-32.55)	-503.12	(-5.39)	-493.84	(3.89)	-497.73
HXeNC-*d*	→	Xe + HCN	-602.64	(-31.91)	-570.25	(0.48)	-566.91	(3.82)	-570.73
HRnCN	→	Rn + HNC	-375.48	(-38.27)	-342.40	(-5.19)	-332.87	(4.34)	-337.21
HRnNC	→	Rn + HCN	-475.91	(-41.13)	-437.91	(-3.13)	-431.55	(3.23)	-434.78
HRnCN-*d*	→	Rn + HNC	-512.64	(-39.85)	-483.31	(-10.52)	-469.28	(3.51)	-472.79
HRnNC-*d*	→	Rn + HCN	-585.20	(-39.07)	-550.62	(-4.49)	-565.49	(-19.36)	-546.13

[a] The values in parentheses are differences with respect to the MP2/zfk4 values: $\mathcal{P}$(MP2/basis) - $\mathcal{P}$(MP2/zfk4)

Table 4.18: Gibbs free energy change (ΔG) and errors in ΔG ($\Delta\Delta G$) with respect to zfk4 values at the PBE0 level of theory.[a] All values are in kJ/mol.

reaction			ims2		ims3		zfk3		zfk4
			ΔG	$\Delta\Delta G$	ΔG	$\Delta\Delta G$	ΔG	$\Delta\Delta G$	ΔG
HCN	→	HNC	50.74	(-2.07)	51.13	(-1.68)	52.94	(0.13)	52.81
HXeCN	→	HXeNC	21.27	(5.36)	14.08	(-1.83)	16.63	(0.72)	15.91
HXeNC	→	HXeCN-*i*	21.44	(6.54)	15.03	(0.13)	14.51	(-0.39)	14.90
HXeCN	→	HXeCN-*i*	42.71	(11.89)	29.11	(-1.71)	31.14	(0.32)	30.82
HXeCN	→	HXeCN-*d*	140.75	(6.47)	128.68	(-5.60)	134.62	(0.34)	134.28
HXeNC	→	HXeNC-*d*	119.47	(0.09)	115.57	(-3.81)	119.02	(-0.36)	119.38
HRnCN	→	HRnNC	23.34	(5.69)	17.59	(-0.06)	18.05	(0.40)	17.65
HRnNC	→	HRnCN-*i*	18.37	(7.14)	12.97	(1.74)	11.10	(-0.13)	11.23
HRnCN	→	HRnCN-*i*	41.71	(12.83)	30.56	(1.68)	29.14	(0.26)	28.88
HRnCN	→	HRnCN-*d*	153.53	(8.57)	147.81	(2.85)	145.36	(0.40)	144.96
HRnNC	→	HRnNC-*d*	130.22	(1.82)	130.98	(2.58)	128.43	(0.03)	128.40
HXeCN	→	Xe + HNC	-393.73	(-16.89)	-391.73	(-14.89)	-377.58	(-0.74)	-376.84
HXeNC	→	Xe + HCN	-465.74	(-20.18)	-456.94	(-11.38)	-447.15	(-1.59)	-445.56
HXeCN-*d*	→	Xe + HNC	-534.48	(-23.36)	-520.41	(-9.29)	-512.19	(-1.07)	-511.12
HXeNC-*d*	→	Xe + HCN	-585.21	(-20.26)	-572.51	(-7.56)	-566.16	(-1.21)	-564.95
HRnCN	→	Rn + HNC	-373.69	(-32.45)	-349.27	(-8.03)	-342.29	(-1.05)	-341.24
HRnNC	→	Rn + HCN	-447.77	(-36.08)	-417.99	(-6.30)	-413.28	(-1.59)	-411.69
HRnCN-*d*	→	Rn + HNC	-527.22	(-41.03)	-497.08	(-10.89)	-487.65	(-1.46)	-486.19
HRnNC-*d*	→	Rn + HCN	-577.99	(-37.90)	-548.97	(-8.88)	-541.71	(-1.62)	-540.09

[a] The values in parentheses are differences with respect to the PBE0/zfk4 values: $\mathcal{P}$(PBE0/basis) - $\mathcal{P}$(PBE0/zfk4)

Table 4.19: Average absolute errors in ΔG with respect to zfk4 values (in kJ/mol).

method	ims2	ims3	zfk3
MP2	18.8	3.7	3.9
PBE0	15.6	5.3	0.7

Reaction rates may be affected by the isotopic substitution which could either increase or decrease the stability of reactants. Table 4.20 shows results for the KIEs in the dissociation (d) and the isomerization (i) reactions. Replacing the hydrogen atom with the heavier deuterium leads to a lower reaction rate in the two-body dissociation and thus in an increased (kinetic) stability of the reagent HRgCN due to the primary KIE (similar to what Khriachtchev *et al.* found for HKrCl [90]). On the other hand, the isomerization reaction is almost unaffected by deuteration, showing only a small inverse secondary isotope effect.

Table 4.20: KIEs (k_D/k_H) for HRgCN at the MP2 level of theory for the HRgCN $\rightarrow$ Rg + HNC dissociation (d) and the HRgCN to HRgNC isomerization (i).

basis sets	HXeCN-d	HRnCN-d	HXeCN-i	HRnCN-i
ims3	0.78	0.78	1.03	1.00
zfk3	0.77	0.80	1.03	1.03
zfk4	0.76	0.79	1.01	1.02

4.4 Conclusion

Excitation energies to the first three excited states with nonzero oscillator strengths were computed for the HRgY systems (Rg = Xe, Rn and Y=CN, NC) at the TDDFT level of theory, using the B2PLYP and B3LYP functionals. Both all-electron (ANO-RCC, Sapporo-TZP-2012, Sapporo-QZP-2012, and QZ4P) and pseudopotential basis sets (IMCP-SR2, IMCP-SR3, ZFK3-DK3, and ZFK4-DK3) were used. For both HRgCN and HRgNC, the most prominent peak in the spectrum is due to the HOMO-LUMO transition and corresponds to the transition $X^1\Sigma^+ \rightarrow 1^1\Sigma^+$. For HRnNC, the HOMO-LUMO transition is its lowest energy transition, occurring at a much lower energy ($\sim$4.5 eV) in the spectrum than that for HRgCN which has its HOMO-LUMO transition occurring at a higher energy ($\sim$6 eV). The splitting relativistic effects (spin-orbit coupling) essentially do not affect the spectra of the HXeY systems. However,

significant shifts occur in the spectra of HRnY systems. For HRnCN, the spin-orbit coupling red-shifted the HOMO-LUMO peak while it blue-shifted the HOMO-LUMO peak for HRgNC. Geometry optimizations carried out for the HRgY systems and their transition states allowed to investigate the efficiency of the new ims3 basis set. The basis set ims3 performed better than ims2, giving results fairly close to the zfk4 reference basis set. The advantage of ims3 is that it is more accurate than ims2 while saving CPU time when compared to zfk3 and zfk4. Lastly, the KIEs were investigated for the two-body dissociation and isomerization reactions. As expected, dissociation slows down when H is replaced by D due to the primary effect, while the isomerization rates remain almost unchanged by the H-D substitution, exhibiting only a minor inverse secondary effect.

Chapter 5

Conclusions & future work

5.1 Conclusions

This work has extended and contributed to the research in the excited states of HRgY type compounds, the effect relativistic effects have on electronic spectra for these systems, and analyzed the performance in terms of accuracy and efficiency of the MCPt and ims3 basis sets in calculations with the HRgY systems. The electronic spectra of HRgF (Rg = Ar-Rn) and HRgY (Rg = Xe, Rn and Y = CN, NC) have been generated by calculating the excited states. It was found that the most prominent peak was due to the HOMO-LUMO transition; the orbitals involved in this transition have σ symmetry. There is a shift of electron density from the F to the H on the HRgF molecules when an electron is transferred from HOMO to LUMO. There is an analogous shift of electron density from the Y group (Y = CN, NC) to the H in the HRgY molecules. The MCP-TZP basis set was found to give similar results for the HRgF compounds while being faster by a a factor of 2.5-3.8 relative to the SAPt basis set. For the HRgY (Rg = Xe, Rn and Y = CN, NC) geometry and thermochemical calculations, it was found that the ims3 basis set performed better than the ims2 basis set, coming much closer to the zfk4 reference basis set while being faster than the zfk3 and zfk4 basis sets. Relativistic effects affected the electronic spectra of the Rn compounds; its HOMO-LUMO peak is red-shifted for all the radon compounds studied except for the HOMO-LUMO peak for HRgNC which is blue-shifted. For

HRgNC, the HOMO-LUMO transition is its lowest energy transition, occurring at a much lower energy (∼4.5 eV) in the spectrum than that for HRgCN which has its HOMO-LUMO transition occurring at a higher energy (∼6 eV).

5.2 Future work

Future work may focus on the higher excited states, triplet states, and the zero oscillator excitations of the HRgCN and HRgNC compounds. More Rn systems may be studied and the splitting relativistic effects in their spectra investigated, analyzing which peaks are red- or blue-shifted and the composition of the orbitals involved. The ims3 basis set may also be refined to make it even more accurate and efficient, especially to design it specifically to work well with excited state calculations on rare gas systems. The spectra of HXeY (where Y = Cl, Br, I) are also of interest as experimental spectra exist for these compounds and would serve as a means to evaluate the improved ism3 basis set.

Bibliography

[1] W. Grochala, "Atypical compounds of gases, which have been called noble," *Chem. Soc. Rev.*, vol. 36, pp. 1632–1655, 2007.

[2] J. Ahokas, K. Vaskonen, J. Eloranta, and H. Kunttu, "Electronic absorption spectra of HXeCl, HXeBr, HXeI, and HXeCN in Xe matrix," *J. Phys. Chem. A*, vol. 104, pp. 9506–9511, 2000.

[3] M. Johansson, M. Hotokka, M. Pettersson, and M. Räsänen, "Quantum chemical potential energy surfaces for HXeCl," *Chem. Phys.*, vol. 244, pp. 25–34, 1999.

[4] G. Audi, F. G. Kondev, M. Wang, W. J. Huang, and S. Naimi, "The NUBASE2016 evaluation of nuclear properties," *Chinese Physics C*, vol. 41, 030 001–(1–138), 2017.

[5] M. Pettersson, J. Lundell, L. Khriachtchev, and M. Räsänen, "Neutral rare-gas containing charge-transfer molecules in solid matrices. III. HXeCN, HXeNC, and HKrCN in Kr and Xe," *J. Chem. Phys.*, vol. 109, pp. 618–625, 1998.

[6] M. D. van Hoeve and M. Klobukowski, "Computational study of the electronic spectra of the rare gas fluorohydrides HRgF (Rg = Ar, Kr, Xe, Rn)," *J. Phys. B: At. Mol. Opt. Phys.*, vol. 51, 055 103–(1 –10), 2018.

[7] T. Zeng and M. Klobukowski, "Practical aspects of computational chemistry I: An overview of the last two decades and current trends," in, J. Leszczynski and M. K. Shukla, Eds. Springer, 2012, ch. 8, pp. 209–254.

[8] L. Pauling, "The formulas of antimonic acid and the antimonates," *J. Am. Chem. Soc.*, vol. 55, pp. 1895–1900, 1933.

[9] N. Bartlett, "Xenon Hexafluoroplatinate(v) $Xe^{+}[PtF_6]^{-}$," *Proc. Chem. Soc.*, p. 218, 1962.

[10] L. Graham, O. Graudejus, N. K. Jha, and N. Bartlett, "Concerning the nature of $XePtF_6$," *Coordination Chemistry Reviews*, vol. 197, pp. 321–334, 2000.

[11] R. Hoppe, W. Dähne, H. Mattauch, and K. Rödder, "Fluorination of xenon," *Angew. Chem. Int. Ed.*, vol. 1, 1962.

[12] H. H. Claassen, H. Selig, and J. G. Malm, "Xenon tetrafluoride," *J. Am. Chem. Soc.*, vol. 84, pp. 3593–3593, 1962.

[13] L. Khriachtchev, M. Räsänen, and R. B. Gerber, "Noble-gas hydrides: New chemistry at low temperatures," *Acc. Chem. Res.*, vol. 42, pp. 183–191, 2009.

[14] L. Khriachtchev, M. Pettersson, N. Runeberg, J. Lundell, and M. Räsänen, "A stable argon compound," *Nature*, vol. 406, pp. 875–876, 2000.

[15] J. Lundell, G. M. Chaban, and R. B. Gerber, "Combined ab initio and anharmonic vibrational spectroscopy calculations for rare gas containing fluorohydrides, HRgF," *Chem. Phys. Lett.*, vol. 331, pp. 308–316, 2000.

[16] Z. Bihary, G. M. Chaban, and R. B. Gerber, "Vibrational spectroscopy and matrix-site geometries of HArF, HKrF, HXeCl, and HXeI in rare-gas solids," *J. Chem. Phys.*, vol. 116, pp. 5521–5529, 2002.

[17] D. R. Hartree, "The wave mechanics of an atom with a non-coulomb central field. Part I. Theory and methods," *Mathematical Proceedings of the Cambridge Philosophical Society*, vol. 24, pp. 89–110, 1928.

[18] D. R. Hartree, "The wave mechanics of an atom with a non-coulomb central field. Part II. Some results and discussion," *Mathematical Proceedings of the Cambridge Philosophical Society*, vol. 24, pp. 111–132, 1928.

[19] J. C. Slater, "The self consistent field and the structure of atoms," *Phys. Rev.*, vol. 32, pp. 339–348, 1928.

[20] J. A. Gaunt, "A theory of Hartree's atomic fields," *Mathematical Proceedings of the Cambridge Philosophical Society*, vol. 24, pp. 328–342, 1928.

[21] V. Fock, "Näherungsmethode zur lösung des quantenmechanischen mehrkörperproblems," *Zeitschrift für Physik*, vol. 61, pp. 126–148, 1930.

[22] D. R. Hartree and W. Hartree, "Self-consistent field, with exchange, for beryllium," *Proc. Chem. Soc. Lond. A.*, vol. 150, pp. 9–33, 1935.

[23] Chr. Møller and M. S. Plesset, "Note on an approximation treatment for many-electron systems," *Phys. Rev. A*, vol. 46, pp. 618–622, 1934.

[24] M. Head-Gordon, J. A. Pople, and M. J. Frisch, "MP2 energy evaluation by direct methods," *Chem. Phys. Lett.*, vol. 153, pp. 503–506, 1988.

[25] J. A. Pople, R. Seeger, and R. Krishnan, "Variational configuration interaction methods and comparison with perturbation theory," *Int. J. Quantum Chem.*, vol. 12, pp. 149–163, 1977.

[26] R. Krishnan and J. A. Pople, "Approximate fourth-order perturbation theory of the electron correlation energy," *Int. J. Quantum Chem.*, vol. 14, pp. 91–100, 1978.

[27] R. G. Parr and W. Yang, *Density-Functional Theory of Atoms and Molecules*. Oxford University Press, 1989.

[28] C. Adamo and V. Barone, "Toward reliable density functional methods without adjustable parameters: The PBE0 model," *J. Chem. Phys.*, vol. 110, pp. 6158–6170, 1999.

[31] J. P. Stephens, F. J. Delvin, C. F. Chabalowski, and M. J. Frisch, "Ab initio calculation of vibrational absorption and circular dichroism spectra using density functional force fields," *J. Phys. Chem.*, vol. 98, pp. 11 623–11 627, 1994.

[32] T. Yanai, D. P. Tew, and N. C. Handy, "A new hybrid exchange–correlation functional using the coulomb-attenuating method (CAM-B3LYP)," *Chem. Phys. Lett.*, vol. 393, pp. 51–57, 2004.

[33] A. Yoshinobu and T. Seiichiro, "Range-separation by the Yukawa potential in long-range corrected density functional theory with Gaussian-type basis functions," *Chem. Phys. Lett.*, vol. 462, pp. 4–6, 2008.

[29] S. Grimme and F. Neese, "Double-hybrid density functional theory for excited electronic states of molecules," *J. Chem. Phys.*, vol. 127, p. 154 116, 2007.

[30] S. Grimme, "Semiempirical hybrid density functional with perturbative second-order correlation," *J. Chem. Phys.*, vol. 124, 034 108–(1–16), 2006.

[35] N. T. Maitra, "Perspective: Fundamental aspects of time-dependent density functional theory," *J. Chem. Phys.*, vol. 144, 220 901–(1–16), 2016.

[36] A. D. Laurent and D. Jacquemin, "TD-DFT benchmarks: A review," *Int. J. Quantum Chem.*, vol. 113, pp. 2019–2039, 2013.

[37] C. C. Lovallo and M. Klobukowski, "Development of new pseudopotential methods: Improved model core potentials for the first-row transition metals," *J. Comput. Chem.*, vol. 24, pp. 1009–1015, 2003.

[38] E. Miyoshi, H. Mori, R. Hirayama, Y. Osanai, T. Noro, H. Honda, and M. Klobukowski, "Compact and efficient basis sets of s- and p-block elements for model core potential method," *J. Chem. Phys.*, vol. 122, 074 104–(1–8), 2005.

[39] T. Zeng and M. Klobukowski, "Model core potentials of p-block elements generated considering the Douglas–Kroll relativistic effects, suitable for accurate spin-orbit coupling calculations," *J. Chem. Phys.*, vol. 133, 114 107–(1–11), 2010.

[40] T. Noro, M. Sekiya, and T. Koga, "Segmented contracted basis sets for atoms H through Xe: Sapporo-(DK)-nZP sets (n = D, T, Q)," *Theor. Chem. Acc.*, vol. 131, pp. 1124–1132, 2012.

[41] T. Noro, M. Sekiya, and T. Koga, "Sapporo-(DKH3)-nZP (n = D, T, Q) sets for the sixth period s-, d-, and p-block atoms," *Theor. Chem. Acc.*, vol. 132, pp. 1363–1368, 2013.

[42] I. Miadoková and V. Kellö, "Standardized basis sets for high-level-correlated relativistic calculations of atomic and molecular electric properties in the spin-averaged Douglas-Kroll approximation," *Theor. Chem. Acc.*, vol. 96, pp. 166–175, 1997.

[43] Z. Benkova, A. J. Sadlej, R. E. Oakes, and S. E. J. Bell, "Reduced-size polarized basis sets for calculations of molecular electric properties. I. the basis set generation," *J. Comput. Chem.*, vol. 26, pp. 145–153, 2005.

[44] R. E. Oakes, S. E. J. Bell, Z. Benkova, and A. J. Sadlej, "Reduced-size polarized basis sets for calculations of molecular electric properties. II. simulation of the raman spectra," *J. Comput. Chem.*, vol. 26, pp. 154–159, 2004.

[45] Z. Benkova, A. J. Sadlej, R. E. Oakes, and S. E. J. Bell, "Reduced–size polarized basis sets for calculations of molecular electric properties. III. second–row atoms," *Theor. Chem. Acc.*, vol. 113, pp. 238–247, 2005.

[46] A. Baranowska, M. Siedlecka, and A. J. Sadlej, "Reduced-size polarized basis sets for calculations of molecular electric properties. IV. first-row transition metals," *Theor. Chem. Acc.*, vol. 118, pp. 959–972, 2007.

[47] E. van Lenthe and E. J. Baerends, "Optimized Slater-type basis sets for the elements 1–118," *J. Comput. Chem.*, vol. 24, pp. 1142–1156, 2003.

[48] M. Jungen, "A Gaussian basis for Rydberg orbitals," *J. Chem. Phys.*, vol. 74, pp. 750–751, 1981.

[49] K. Kaufmann, W. Baumeister, and M. Jungen, "Universal Gaussian basis sets for an optimum representation of Rydberg and continuum wavefunctions," *J. Phys. B: At. Mol. Opt. Phys.*, vol. 22, pp. 2223–2240, 1989.

[50] S. Huzinaga and M. Klobukowski, "Well-tempered GTF basis sets for the atoms K through Xe," *Chem. Phys. Lett.*, vol. 120, pp. 509–512, 1985.

[51] P. Atkins and J. de Paula, *Atkins' Physical Chemistry*, 10th ed. Oxford University Press, 2014.

[52] M. W. Schmidt, K. K. Baldridge, J. A. Boatz, S. T. Elbert, M. S. Gordon, J. H. Jensen, S. Koseki, N. Matsunaga, K. A. Nguyen, S. Su, T. L. Windus, M. Dupuis, and J. J. A. Montgomery, "General atomic and molecular electronic structure system," *J. Comput. Chem.*, vol. 14, pp. 1347–1363, 1993.

[53] F. Neese, "The ORCA program system," *Wiley Interdisciplinary Reviews: Computational Molecular Science*, vol. 2, pp. 73–78, 2012.

[54] F. Neese, "Software update: The ORCA program system, version 4.0," *Wiley Interdisciplinary Reviews: Computational Molecular Science*, vol. 8, e1327, 2018.

[55] "ADF Program System," Scientific Computing and Modelling NV, Vrije Universiteit, Theoretical Chemistry, De Boelelaan 1083, 1081 HV Amsterdam, The Netherlands, Tech. Rep., 2000.

[56] M. Pettersson, L. Khriachtchev, A. Lignell, and Z. Bihary, "HKrF in solid krypton," *J. Chem. Phys.*, vol. 116, pp. 2508–2515, 2002.

[57] G. M. Chaban, J. Lundell, and R. B. Gerber, "Theoretical study of decomposition pathways for HArF and HKrF," *Chem. Phys. Lett.*, vol. 364, pp. 628–633, 2002.

[58] Y. Chen and W. Hu, "Rate constant calculation for HArF $\rightarrow$ Ar + HF and HKrF $\rightarrow$ Kr + HF reactions by dual-level variational transition state theory with quantized reactant state tunneling," *J. Phys. Chem. A*, vol. 108, pp. 4449–4454, 2004.

[59] A. V. Bochenkova, V. E. Bochenkov, and L. Khriachtchev, "HArF in solid argon revisited: Transition from unstable to stable configuration," *J. Phys. Chem. A*, vol. 113, pp. 7654–7659, 2009.

[60] L. Khriachtchev, M. Pettersson, A. Lignell, and M. Räsänen, "A more stable configuration of HArF in solid argon," *J. Am. Chem. Soc.*, vol. 123, pp. 8610–8611, 2001.

[61] A. Lignell, M. Räsänen, and L. Khriachtchev, "Formation of HArF in solid Ar revisited: Are mobile vacancies involved in the matrix-site conversion at 30 K?" *J. Chem. Phys.*, vol. 120, pp. 3353–3357, 2004.

[62] S. Jolkkonen, M. Pettersson, and J. Lundell, "Trapping site structures of HArF and HKrF in solid rare gases," *J. Chem. Phys.*, vol. 119, pp. 7356–7364, 2003.

[63] R. B. Gerber, "Formation of novel rare-gas molecules in low-temperature matrices," *Annu. Rev. Phys. Chem.*, vol. 55, pp. 55–78, 2004.

[64] A. Fitzsimmons, H. Mori, E. Miyoshi, and M. Klobukowski, "Model core potential and all-electron studies of molecules containing rare gas atoms," *J. Phys. Chem. A*, vol. 114, pp. 8786–8792, 2010.

[65] A. Fitzsimmons and M. Klobukowski, "Basis set effects in simple compounds of heavy rare gases," *Can. J. Chem.*, vol. 91, pp. 894–901, 2013.

[66] S. Huzinaga, M. Klobukowski, and Y. Sakai, "Model potential method in molecular calculations," *J. Phys. Chem.*, vol. 88, pp. 4880–4886, 1984.

[67] M. Klobukowski, S. Huzinaga, and Y. Sakai, "Model core potentials: Theory and applications," in *Computational Chemistry: Reviews of Current Trends*, J. Leszczynski, Ed., vol. 3, World Scientific, Singapore, 1999, p. 49.

[68] V. Bonifacic and S. Huzinaga, "Atomic and molecular calculations with the model potential method. I," *J. Chem. Phys.*, vol. 60, pp. 2779–2786, 1974.

[69] M. E. Casida, C. Jamorski, K. C. Casida, and D. R. Salahub, "Molecular excitation energies to high-lying bound states from time-dependent density functional response theory: Characterization and correction of the time-dependent local density approximation ionization threshold," *J. Chem. Phys.*, vol. 108, pp. 4439–4449, 1998.

[70] A. Dreuw and M. Head-Gordon, "Single-reference ab initio methods for the calculation of excited states of large molecules," *Chem. Rev.*, vol. 105, pp. 4009–4037, 2005.

[71] R. Weber, B. Hovda, and G. Schoendorff, "Behavior of the Sapporo-nZP-2012 basis set family," *Chem. Phys. Lett.*, vol. 637, pp. 120–126, 2015.

[72] B. A. Hess, "Relativistic electronic-structure calculations employing a two-component no-pair formalism with external-field projection operators," *Phys. Rev. A*, vol. 33, pp. 3742–3748, 1986.

[73] G. Jansen and B. A. Hess, "Revision of the Douglass-Kroll transformation," *Phys. Rev. A*, vol. 39, pp. 6016–6017, 1989.

[74] D. G. Henshaw, "Atomic distribution in liquid and solid neon and solid argon by neutron diffraction," *Phys. Rev.*, vol. 111, pp. 1470–1475, 1958.

[75] K. Mendelssohn, M. Ruhemann, and F. Simon, *Z. Physik. Chem.*, vol. B15, p. 389, 1931.

[76] K. Hakuta, S. Miki, and H. Takuma, "Photoabsorption cross-section measurement of Ar_2F excimer at 248 nm," *J. Opt. Soc. Am. B*, vol. 5, pp. 1261–1265, 1988.

[77] D. B. Geohegan and J. G. Eden, "Xe_2Cl and Kr_2F excited state absorption spectra: Measurements of absolute cross sections," *Chem. Phys. Lett.*, vol. 139, pp. 519–524, 1987.

[78] C. Bressler, W. G. Lawrence, and N. Schwentner, "Spectroscopy of argon fluoride and krypton fluoride exciplexes in rare gas matrices," *J. Chem. Phys.*, vol. 105, pp. 10 178–10 188, 1996.

[79] A. Rosa, E. J. Baerends, S. J. A. van Gisbergen, E. van Lenthe, J. A. Groeneveld, and J. G. Snijders, "Electronic spectra of $M(CO)_6$ (M = Cr, Mo, W) revisited by a relativistic TDDFT approach," *J. Am. Chem. Soc.*, vol. 121, pp. 10 356–10 365, 1999.

[80] P. Romaniello, M. C. Aragoni, M. Arca, T. Cassano, C. Denotti, F. A. Devillanova, F. Isaia, F. Lelj, V. Lippolis, and R. Tommasi, "Ground and excited states of $[M(H_2timdt)_2]$ neutral dithiolenes (M = Ni, Pd, Pt; H_2timdt) monoanion of imidazolidine-2,4,5-trithione): Description within TDDFT and scalar relativistic (ZORA) approaches," *J. Phys. Chem. A*, vol. 107, pp. 9679–9687, 2003.

[81] G. te Velde, F. M. Bickelhaupt, E. J. Baerends, C. Fonseca Guerra, S. J. A. van Gisbergen, J. G. Snijders, and T. Ziegler, "Chemistry with ADF," *J. Comput. Chem.*, vol. 22, no. 9, pp. 931–967, 2001, ISSN: 1096-987X. DOI: 10.1002/jcc.1056. [Online]. Available: http://dx.doi.org/10.1002/jcc.1056.

[82] E. J. Baerends, T. Ziegler, A. J. Atkins, J. Autschbach, D. Bashford, O. Baseggio, A. Bérces, F. M. Bickelhaupt, C. Bo, P. M. Boerritger, L. Cavallo, C. Daul, D. P. Chong, D. V. Chulhai, L. Deng, R. M. Dickson, J. M. Dieterich, D. E. Ellis, M. van Faassen, A. Ghysels, A. Giammona, S. J. A. van Gisbergen, A. Goez, A. W. Götz, S. Gusarov, F. E. Harris, P. van den Hoek, Z. Hu, C. R. Jacob, H. Jacobsen, L. Jensen, L. Joubert, J. W. Kaminski, G. van Kessel, C. König, F. Kootstra, A. Kovalenko, M. Krykunov, E. van Lenthe, D. A. McCormack, A. Michalak, M. Mitoraj, S. M. Morton, J. Neugebauer, V. P. Nicu, L. Noodleman, V. P. Osinga, S. Patchkovskii, M. Pavanello, C. A. Peeples, P. H. T. Philipsen, D. Post, C. C. Pye, H. Ramanantoanina, P. Ramos, W. Ravenek, J. I. Rodríguez, P. Ros, R. Rüger, P. R. T. Schipper, D. Schlüns, H. van Schoot, G. Schreckenbach, J. S. Seldenthuis, M. Seth, J. G. Snijders, M. Solà, S. M., M. Swart, D. Swerhone, G. te Velde, V. Tognetti, P. Vernooijs, L. Versluis, L. Visscher, O. Visser, F. Wang, T. A. Wesolowski, E. M. van Wezenbeek, G. Wiesenekker, S. K. Wolff, T. K. Woo, and A. L. Yakovlev, *ADF2017, SCM, Theoretical Chemistry, Vrije Universiteit, Amsterdam, The Netherlands, https://www.scm.com.*

[83] M. Seth and T. Ziegler, "Range-separated exchange functionals with Slater-type functions," *J . Chem. Theory Comput.*, vol. 8, pp. 901–907, 2012.

[84] E. van Lenthe, E. J. Baerends, and J. G. Snijders, "Relativistic regular two-component Hamiltonians," *J. Chem. Phys.*, vol. 99, pp. 4597–4610, 1993.

[85] E. van Lenthe, E. J. Baerends, and J. G. Snijders, "Relativistic total energy using regular approximations," *J. Chem. Phys.*, vol. 101, pp. 9783–9792, 1994.

[86] E. van Lenthe, R. van Leeuwen, E. J. Baerends, and J. G. Snijders, "Relativistic regular two-component Hamiltonians," *Int. J. Quantum Chem.*, vol. 57, pp. 281–293, 1996.

[87] E. van Lenthe, J. G. Snijders, and E. J. Baerends, "The zero-order regular approximation for relativistic effects: The effect of spin–orbit coupling in closed shell molecules," *J. Chem. Phys.*, vol. 105, pp. 6505–6516, 1996.

[88] M. Douglas and N. M. Kroll, "Quantum electrodynamical corrections to the fine structure of helium," *Ann. Phys.*, vol. 82, pp. 89–115, 1974.

[89] R. Juarez, C. Zavala-Oseguera, J. O. C. Jimenez-Halla, F. M. Bickelhaupt, and G. Merino, "Radon hydrides: Structure and bonding," *Phys. Chem. Chem. Phys.*, vol. 13, pp. 2222–2227, 2011.

[90] L. Khriachtchev, M. Saarelainen, M. Pettersson, and M. Räsänen, "H/D isotope effects on formation and photodissociation of HKrCl in solid Kr," *J. Chem. Phys.*, vol. 118, pp. 6403–6410, 2003.

[91] S. Berski, Z. Latajka, B. Silvi, and J. Lundell, "Electron localization function studies of the nature of binding in neutral rare-gas containing hydrides: HKrCN, HKrNC, HXeCN, HXeNC, HXeOH, and HXeSH," *J. Chem. Phys.*, vol. 114, pp. 4349–4358, 2001.

[92] G. Zhang, S. Zhang, and D. Chen, "Long-bonding in HNgCN/NC (Ng = Noble Gas) molecules: An NBO/NRT investigation," *J. Phys. Chem. A*, vol. 121, pp. 5524–5532, 2017.

[93] G. Zhang, J. Song, L. Fu, K. Tang, Y. Su, and D. Chen, "Understanding and modulating the high-energy properties of noble-gas hydrides from their long-bonding: An NBO/NRT investigation on $HNgCO^+/CS^+/OSi^+$ and HNgCN/NC (Ng = He, Ar, Kr, Xe, Rn) molecules," *Phys. Chem. Chem. Phys.*, vol. 20, pp. 10 231–10 239, 2018.

[94] A. D. Becke, "Density-functional thermochemistry. I. The effect of the exchange-only gradient correction," *J. Chem. Phys.*, vol. 96, pp. 2155–2160, 1992.

[95] A. D. Becke, "Density-functional thermochemistry. II. The effect of the Perdew–Wang generalized-gradient correlation correction," *J. Chem. Phys.*, vol. 97, pp. 9173–9177, 1992.

[96] A. D. Becke, "Density-functional thermochemistry. III. The role of exact exchange," *J. Chem. Phys.*, vol. 98, pp. 5648–5652, 1993.

[97] C. Lee, W. Yang, and R. G. Parr, "Development of the Colle-Salvetti correlation-energy formula into a functional of the electron density," *Phys. Rev. B*, vol. 37, pp. 785–789, 1988.

[98] B. O. Roos, R. Lindh, P. Å. Malmqvist, V. Veryazov, and P. O. Widmark, "Main group atoms and dimers studied with a new relativistic ANO basis set," *J. Phys. Chem.*, vol. 108, pp. 2851–2858, 2004.